

SURFACE EFFECTS IN STANNIC OXIDE CRYSTALS

By

JAMES EDWARD HURT

Bachelor of Science  
Oklahoma State University  
Stillwater, Oklahoma  
1957

Master of Science  
Oklahoma State University  
Stillwater, Oklahoma  
1959

Submitted to the Faculty of the Graduate School of  
the Oklahoma State University  
in partial fulfillment of the requirements  
for the degree of  
DOCTOR OF PHILOSOPHY  
May, 1963

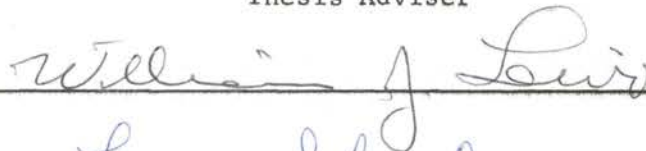
JAN 8 1964

SURFACE EFFECTS IN STANNIC OXIDE CRYSTALS

Thesis Approved:



Thesis Adviser











Dean of the Graduate School

This research was supported by the  
Office of Naval Research under  
Contract No. Nonr-2595(01)

#### ACKNOWLEDGMENT

The author wishes to express his deepest gratitude to Dr. E. E. Kohnke for his valuable guidance throughout the execution of this work, to the Office of Naval Research for sponsoring this research, and to the Oklahoma State University Research Foundation for their support. A note of thanks is also due a number of members of the physics faculty for their encouragement and to Dr. G. B. Thurston, Professor C. F. Harris, and M. D. Bell for the loan of equipment. He is also indebted to J. W. Northrip II, J. E. Houston, E. E. Tolly, and A. J. Belski for their helpful discussions and/or assistance in carrying out certain experimental procedures, to H. F. Kunkle, Jr., for the preparation and furnishing of the artificial crystals, and to H. Hall and F. Hargrove for the construction of experimental apparatus and the mechanical preparation of natural samples suitable for optical and electrical measurements.

## TABLE OF CONTENTS

Chapter	Page
I. INTRODUCTION . . . . .	1
Statement of the Problem . . . . .	1
Stannic Oxide . . . . .	2
Surface Effects in Oxides . . . . .	3
II. THEORETICAL BACKGROUND . . . . .	7
Surface States . . . . .	7
Photoconduction . . . . .	8
Chemisorption and Photoconduction Kinetics for Zinc Oxide . . . . .	10
III. SAMPLES, APPARATUS, AND EXPERIMENTAL METHODS . . . . .	19
Natural Samples . . . . .	19
Artificial Samples . . . . .	21
Sample Cleaning and Contact Materials . . . . .	22
Apparatus for Effect of Ambient on Photoconductivity . . . . .	23
Measurement of Ambient Effect on Photoconductivity . . . . .	25
Apparatus for Effect of Temperature on Photocon- ductivity . . . . .	30
Measurement of Temperature Effect on Photoconduc- tivity . . . . .	32
Measurement of Ambient Effect on Dark Conductivity . . . . .	33
Contact Potential Measurements . . . . .	34
Oxidation and Reduction . . . . .	34
Wavelength Dependence of Photoconductivity . . . . .	35
Other Experimental Work . . . . .	36
IV. RESULTS . . . . .	38
Introductory Statements . . . . .	38
Initial Photoconductivity Calculations . . . . .	38
Effect of Ambient on Photoconductivity . . . . .	40
Effect of Temperature on Photoconductivity . . . . .	58
Oxidation and Reduction . . . . .	68
Effect of Ambient on Dark Conductivity and Contact Potential . . . . .	74
Wavelength Dependence of Photoconductivity . . . . .	75
Effects of Indium Diffusion . . . . .	77
Other Work . . . . .	78
V. DISCUSSION AND CONCLUSIONS . . . . .	80
Summary of Results . . . . .	80
The Photoconduction Kinetics in Terms of a Chemisorption Process . . . . .	82

Effects of Oxidation and Reduction . . . . .	102
Effects of Indium Diffusion . . . . .	102
Suggestions for Further Study . . . . .	103
BIBLIOGRAPHY . . . . .	108

LIST OF TABLES

Table	Page
I. Appearance and Dark Conductivity of Natural Samples . . .	22
II. Effect of Oxygen on Decay Parameters of Sample XVII . . .	48
III. Effect of Admitting Air at Several Temperatures (Sample XIII A) . . . . .	51
IV. Comparison of Photoconductive Response in Air and Vacuum in Sample XIII A at 325°K . . . . .	50
V. Effect of Ambient on Response of Sample III . . . . .	52
VI. Effect of Ambient on Photoresponse of Sample XVII . . . .	54
VII. Effect of Ambient on Photoresponse of Sample IV . . . . .	54
VIII. Effect of Ambient on Photoresponse of Artificial Samples Having Roughened Surfaces . . . . .	57
IX. Comparison of Photocurrent Decays at Low Temperature . .	64
X. Decay Parameters of Sample IV in Air . . . . .	66
XI. Parameters Associated With the Onset of Sublinearity in Logarithmic Decay Curves . . . . .	67
XII. Results of Oxidation and Reduction Experiments . . . . .	70
XIII. Typical Rise and Decay Parameters of Sample VIII B Following Reduction in Vacuum . . . . .	73
XIV. Contact Potential Measurements for Sample VII . . . . .	74
XV. Parameters Associated With Calculation of B (Sample IV) .	90
XVI. Variation of F and S for Sample GI at 190°K . . . . .	97

## LIST OF FIGURES

Figure	Page
1. Surface Energy Level Diagram . . . . .	12
2. Block Diagram of Vacuum System . . . . .	24
3. High Vacuum Sample Holder . . . . .	26
4. Low Temperature Sample Holder . . . . .	31
5. Typical Photocurrent Rise Curves for a Natural Sample . . .	41
6. Typical Photocurrent Decay Curves for a Natural Sample . . .	43
7. Logarithmic Decay Curves for a Natural Sample . . . . .	44
8. Effect of Removal of Air on Photocurrent Rise . . . . .	45
9. Effect of Admitting Air on Photocurrent Decay . . . . .	46
10. Effect of Oxygen Admission on Decay . . . . .	47
11. Effect of Admission of Air on Logarithmic Decay at Low Temperature . . . . .	49
12. Typical Rise and Decay of Photocurrent for an Artificial Sample . . . . .	56
13. Photoresponse vs Temperature . . . . .	59
14. Logarithmic Decays for Sample IV at Several Temperatures . .	60
15. Logarithmic Decays for Sample XIII A at Several Temperatures	62
16. Typical Rise and Decay Curves for a Natural Sample at Low Temperatures . . . . .	63
17. Effect of Temperature on Photocurrent Decay in a Typical Artificial Sample . . . . .	69
18. Effects of Reduction and Surface Abrasion on Decay in Sample VIII B . . . . .	72
19. Photoresponse vs Wavelength for Artificial Samples . . . . .	76
20. Influence of Photoconduction on Surface Energy Bands in Stannic Oxide . . . . .	100



## CHAPTER I

### INTRODUCTION

#### Statement of the Problem

In the investigation of electrical properties of semiconducting solids, results are usually obtained which reflect a composite of bulk and surface characteristics. That the surface properties should differ from those of the bulk is a direct consequence of the boundary value nature of the problem. Inasmuch as surface properties often control the electrical behavior of a semiconductor, it is desirable to perform experiments which separate surface effects from those of the bulk and define the nature and extent of the difference.

Although a theoretical basis for the existence of electronic energy states unique to the surface regions of semiconducting or insulating crystalline materials has been known since shortly after the advent of quantum mechanics, the investigation of these states and their effects in various materials has become of appreciable interest only during the last fifteen years. The materials most intensely studied, owing to their applications in electronics, are the semiconducting elements germanium and silicon. (1-8).

Still more recently, the discovery that the performance of certain photoconducting oxides is linked directly with adsorption phenomena has resulted in an intensified interest in the surface properties of compound semiconductors. Among the oxides in which such effects have

been noted are titanium dioxide, lead monoxide, and zinc oxide. (9-16).

The present study will be concerned with the relationship of surface processes to the electrical properties of monocrystalline samples of stannic oxide.

### Stannic Oxide

Stannic oxide, the chemical formula for which is  $\text{SnO}_2$ , is one of a number of oxides and fluorides having the bipyramidal ditetragonal crystal structure commonly referred to as the rutile structure. The lattice dimensions are  $a = 4.72 \text{ \AA}$  and  $c = 3.16 \text{ \AA}$ , giving a  $c/a$  ratio of 0.6695. This substance occurs naturally as the mineral cassiterite, and is very stable chemically, resisting action by the strongest of acids and being readily decomposed only by hot solutions of sodium hydroxide or potassium hydroxide. It is soluble only in certain oxides at temperatures above the melting points of these oxides and cannot be obtained in a liquid state at ordinary pressures, decomposing from the solid phase above  $1600^\circ\text{C}$ .

For these reasons, the growth of artificial single crystals of a size suitable for laboratory work has proved to be a somewhat elusive process. The preparation of microscopic stannic oxide crystals by heating stannic oxide powder in a stream of hydrogen chloride gas was reported more than a century ago by Deville (17), but only recently has the growth of macroscopic single crystals been accomplished. (18). A vapor phase technique was employed.

Virtually all published work describing the optical and electrical properties of this material has therefore involved either natural specimens, thin polycrystalline films, or pressed powders. Several studies of the optical absorption and electrical conductivity have

been reported, with resulting values of the forbidden energy gap ranging from about 3.3 eV to 4.1 eV. (19-23). As a rule, the higher values were obtained in measurements of conductivity at high temperatures, while the lower values came from measurements of the fundamental optical absorption edge. However, Ishiguro, et al (23), report a value near 4 eV from room temperature optical measurements on thin films.

The semiconducting properties of many of the natural samples which were used in this study had previously been investigated. Room temperature optical absorption edge values corresponding to band gap values of 3.45 eV and 3.47 eV have been reported by Northrip (24) and Belski (25), respectively. Electrical conductivity has been measured by Northrip (24) and Tolly (26), Hall mobility and carrier density by Tolly (26), and photoconductive response by Hurt (27). Although no detailed picture of the conduction mechanism in these samples can be presented on the basis of measurements to date, a broad-band model with the possibility of some impurity band conduction is favored. (28). In this respect, then, stannic oxide may resemble materials such as zinc oxide more closely than the structurally similar rutile form of titanium dioxide, which is characterized by conduction in a narrow 3d-band. (29).

Specific properties of the samples used will be discussed in Chapter III. For a review of the earlier investigations of the properties of stannic oxide and materials of related interest the reader is referred to Northrip (24).

#### Surface Effects in Oxides

The effects of primary interest are those in which interactions

of the surface with the surrounding gaseous ambient produce alterations in the electrical properties of the oxide. This usually involves sorption phenomena, which are concerned with the attachment of atoms, molecules, or ions of the ambient to the surface and their detachment from the surface. There are two general types of adsorption. These are physical adsorption, in which case the adsorbed atom or molecule is attached by short-range cohesive or adhesive forces and retains its form as an atom or molecule, and chemisorption, in which case there is a sharing or transfer of electrons between the solid and the adsorbed species.

If there is an electron transfer, the height of the surface potential barrier varies with the density of chemisorbate. Because of the control which the surface space charge layer may hold over the behavior of the solid as a whole, the consequences of these ambient effects can be detected by measurements which are not limited strictly to the surface. Surface effects due to chemisorption, then, can be expected to show up in measurements of conductivity and photoconductivity as well as in those of field effect and contact potential.

Such effects have been measured in several oxides, that of zinc being the most extensively examined. Miller (12) reviews chemisorption effects in this material, while Morrison (13) discusses the related surface barrier effects. Melnick (14), using sintered samples, has shown that the zinc oxide photoconduction process is intimately associated with oxygen chemisorption and has developed a quantitative treatment for the kinetics of photoconduction and chemisorption based on the assumption that the rate-limiting process is the transfer of charge at the surface on which chemisorption takes place. This

treatment has been verified and extended by Medved (16), and will be discussed in some detail in the following chapter. Collins and Thomas (15) have studied the photoconductivity of single crystals of zinc oxide in various ambients, finding that both oxygen and a mixture of oxygen and water vapor tend to inhibit photoconduction, the latter to a greater extent. These latter investigators have advanced the theory that the photoconduction seen in zinc oxide originates entirely at the surface, with both chemisorbed oxygen and lattice oxygen acting as hole-trapping centers. Krusemeyer (30) has measured the contact potential, surface conductivity, and field effect mobility at room temperature in single crystals of zinc oxide in both oxygen and a vacuum of  $10^{-6}$  mm Hg. His results, in connection with some of those of Collins and Thomas (15), indicate a surface hole-trapping quantum efficiency of approximately unity for a neutral surface.

The proposed photoconduction mechanism in zinc oxide is one in which the basic processes are, first, the production of a hole-electron pair by an incident ultraviolet photon and, second, the trapping of the hole at the surface to neutralize and desorb an oxygen ion and leave the corresponding electron in the conduction band. The work of Collins and Thomas (15) has shown that in single crystals not only are adions desorbed, but that a continuation of oxygen desorption takes place as photolysis of the surface.

A similar dependence of photoconduction on ambient oxygen has been reported in rhombic lead monoxide by Bigelow and Haq (11), who have suggested that a mechanism of the same type as that in zinc oxide is operative in this oxide. Similar results have been obtained by Izvozhikov (10) in polycrystalline samples of lead monoxide

(structure not specified).

Kennedy and coworkers (9) have reported results of an entirely different nature in polycrystalline samples of titanium dioxide, both the anatase and rutile structures having been investigated. In both crystalline forms, the incident light was seen to promote adsorption, as opposed to the desorption observed in zinc oxide. The photoconduction of rutile single crystals has been examined by Cronmeyer (31), but without any search for ambient effects.

It is the purpose of the present study to report results of an initial survey of the surface properties of single crystals of stannic oxide, a rutile-structure broad-band semiconductor, and to propose a photoconduction mechanism for this material. The experimental work involved consists of measurements of photoconductivity as a function of ambient and temperature, measurements of conductivity and contact potential as a function of ambient, plus an examination of certain effects of oxidation, reduction, and the introduction of a trivalent impurity. It is hoped that the results obtained will lead to a more thorough understanding of this oxide and serve as guideposts in future studies of this and similar materials, as well as suggest applications in catalysis and other related fields.

## CHAPTER II

### THEORETICAL BACKGROUND

#### Surface States

During the early development of quantum mechanics a method for calculating the wave functions associated with a periodic potential was devised by Kronig and Penney (32). Their one-dimensional method was of conceptual usefulness to those who were interested in the behavior of electrons in crystalline solids, since a crystal structure, with its regular arrangement of ions or atoms, must have a periodically varying potential along any straight line through it. The infinite sequence of square potential wells of finite depth treated by the above theoreticians, then, provided a first-order approximation to the case of an electron within the bulk of a crystal. Tamm (33) modified this basic model by affixing a boundary, with the result that electron energy levels at and near the boundary were predicted which were forbidden within the bulk. In the case of an insulating or semiconducting crystal, this predicted surface states between the valence band and the conduction band. Such states have since been referred to as "Tamm states."

These surface states were given further consideration by several investigators, among them Shockley (34), who calculated the surface states for a periodic potential having an arbitrary form of the potential function and discussed the extension of the one-dimensional

model to three dimensions. In accounting for effects observed in rectification studies using germanium and silicon, Bardeen (35) proposed additional sources of surface states in surface defects and foreign atoms, and as a direct result of charged surface states the existence of a surface space charge region to a depth of from  $10^{-6}$  cm to  $10^{-4}$  cm. Bardeen's work showed that the surface properties of a semiconductor could be a critical and often unpredictable factor in the material's over-all behavior. Only in recent years have techniques been developed with which atomically clean surfaces can be studied and the highly idealized theoretical conditions more nearly approached. Work on clean germanium surfaces has been reviewed by Handler (2).

#### Photoconduction

Photoconduction is the process by which the electrical conductivity of a material is enhanced through action of incident light energy. In its intrinsic form, this process involves the production of a hole-electron pair by absorption of a photon having an energy at least equal to the width of the forbidden gap between the valence band and the conduction band. The electron enters the conduction band, leaving the hole in the valence band, so that two current carriers can be added by the absorption of a single photon. In practice, this picture is complicated by the existence of localized states within the forbidden gap which can act as trapping or recombination centers. These centers determine the sign of the majority photocurrent carrier and the lifetime of this carrier. These energy states may include surface states as well as those within the bulk of the material.



Should surface states constitute an appreciable fraction of the trapping and/or recombination centers, then one might expect to see an influence of surface phenomena on photoconductive behavior.

The conductivity of a solid can be expressed as the product

$$\sigma = ne\mu \quad (1)$$

where  $n$  is the volume density of carriers,  $e$  is the charge of one carrier, and  $\mu$  is the mobility of a typical carrier, i.e. the velocity per unit electric field intensity acquired as a result of the application of the field. These quantities are dependent upon the energy levels associated with impurities and other lattice imperfections and may show marked variations between the interior and the surface of a single piece of material. Photoconduction is customarily regarded as a process in which the carrier density is the quantity altered, mobility remaining constant.

In a number of materials the peak photosensitivity and a sharp onset of optical absorption can be seen to coincide on an optical wavelength or energy scale. This indicates that the photons absorbed are contributing to photoconduction, and in a simple photoconductor such an energy value would be a measure of the band gap. If the absorption coefficient is sufficiently great, many of the photocurrent carriers will be produced quite close to the surface, so that surface states and the associated space charge layer can noticeably influence these carriers.

These general considerations have been found to apply to a number of photoconducting oxides. A prime example is zinc oxide, which may constitute an extreme case in that there is evidence indicating that the photoconduction is determined entirely by the surface. (15)

Chemisorption and Photoconduction Kinetics  
for Zinc Oxide

Morrison (13) has proposed a chemisorption mechanism in which electron transfer over the surface barrier is the rate-limiting process to explain the variation of conductivity of zinc oxide as a function of temperature. Using this model, Melnick (14) developed the photoconduction kinetics for zinc oxide, quantitatively demonstrating the relationship between chemisorption and photoconduction in sintered samples of this compound. In further work on sintered zinc oxide, Medved (16) has obtained results similar to those of Melnick (14) and has derived an applicable equation of the Elovich type to describe the electron transfer at the surface barrier. The essential elements of this treatment follow.

It is first necessary to make the following simplifying assumptions:

1. Holes generated by photon absorption either recombine with conduction electrons or migrate to the surface in a time very short compared to that involved in the basic rate-limiting process, so that the direct contribution of holes to photoconduction is negligible.
2.  $\Delta n/n \gg \Delta q/q$ , where  $n$  is the volume density of conduction electrons and  $q$  is the surface concentration of the chemisorbed species.
3. Processes governing physical adsorption act rapidly in comparison with the basic rate-limiting process.
4.  $\Delta N = \Delta Q$ , where  $\Delta N$  is the change in the total number of conduction electrons and  $\Delta Q$  is the change in the total

number of chemisorbed oxygen ions.

The rate equation for chemisorption can now be written in the form

$$\frac{dq_c}{dt} = sq_p \eta_e - \zeta q_c - L \quad (2)$$

where  $q_c$  and  $q_p$  are surface concentrations of chemisorbed and physically adsorbed oxygen respectively,  $s$  is the capture cross section of the physically adsorbed species for an electron on the surface,  $\eta_e$  is the number of conduction electrons penetrating each square centimeter of the surface barrier per second,  $\zeta$  is the rate of desorption due to thermal excitation, and  $L$  is the photodesorption rate term. The barrier penetration process is fundamentally the same as that of thermionic emission, so  $\eta_e$  can be calculated using the Richardson-Dushman equation. Therefore,

$$\eta_e \doteq n\bar{v}(T) \exp[-E(q_c)/kT] \quad (3)$$

where  $n$  is as above,  $\bar{v}(T)$  is the averaged thermal velocity of the conduction electrons,  $E(q_c)$  is the energy height of the surface barrier,  $k$  is Boltzmann's constant, and  $T$  is the absolute temperature. With negative charge held at the surface by chemisorbed oxygen ions, the surface barrier should consist of a "depletion layer," i.e., a space charge layer in which the density of conduction electrons is reduced because of electrostatic repulsion from the negatively charged surface. Such a barrier layer is shown schematically in Figure 1, with the barrier height  $E(q_c)$  and the "chemisorption binding energy"  $E_c$  indicated.

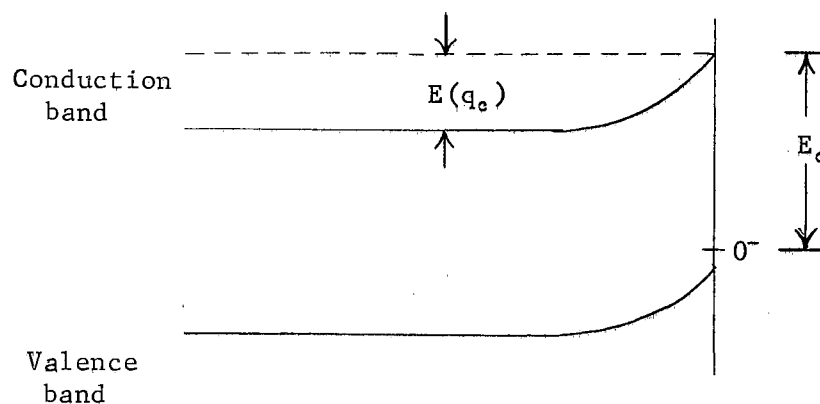


Figure 1. Surface Energy Level Diagram

$E_c$  is much larger than  $E(q_c)$  for all values of  $q_c$ . Binding energies for chemisorption are usually in the range between one and three electron volts. Since  $E_c$  can be considered to be much greater than any thermal energies to be dealt with here, the second term in Equation 2 is negligible. Thermal energies of interest will have an upper limit of about 0.032 eV. Equation 2 can now be written

$$\frac{dq_c}{dt} = sq_p n \bar{v}(T) \exp[-E(q_c)/kT] \quad (4a)$$

for the case in which there is no incident illumination of sufficient energy to initiate photodesorption and

$$\frac{dq_c}{dt} = sq_p n \bar{v}(T) \exp[-E(q_c)/kT] - L \quad (4b)$$

for the case in which photodesorption occurs.

Letting  $a'(P,T) = s(T)\bar{v}(T)q_p(P,T)$  and dropping the subscript  $c$ , Equations 4a and 4b become

$$\frac{dq}{dt} = a'(P,T)n \exp[-E(q)/kT] \quad (5a)$$

and

$$\frac{dq}{dt} = a'(P,T)n \exp[-E(q)/kT] - L \quad (5b)$$

Let the barrier layer have a thickness  $d$  and a dielectric permittivity  $\kappa$ , and assume a uniform donor density. The barrier layer arises from negative charge held in the surface trapping levels associated with chemisorbed oxygen, the areal density of which is  $q$ . If  $\rho$  is the positive charge density in the barrier layer,  $\Phi$  is potential difference, and  $x$  is the coordinate representing the linear distance measured from the surface and positive toward the interior of the solid, the appropriate form of the one-dimensional Poisson equation is

$$\frac{\partial^2 \Phi}{\partial x^2} = -\rho/\kappa \quad (6)$$

Integrating twice between the limits  $x = 0$  and  $x = d$  gives  $\Phi = -\rho d^2/2\kappa$ , which corresponds to a barrier energy height of

$$E(q) = -e\Phi = \rho d^2 e/2\kappa \quad (7)$$

The negative charge per unit surface area is  $-eq$ , so the positive charge per unit volume in the barrier layer is  $\rho = eq/d$ . Substituting this into Equation 7 gives

$$E(q) = e^2 qd/2\kappa = e^2 q/C_a \quad (8)$$

where  $C_a$  is the capacitance of the barrier layer per unit area independent of  $q$ .

The quantity  $C_a$  is a constant if the second initial assumption is fulfilled. Letting  $a'(P,T)n = a(P,T)$  and  $e^2/C_a kT = b(T)$ , the chemisorption rate equations become

$$\frac{dq}{dt} = a \exp(-bq) \quad (9a)$$

and

$$\frac{dq}{d\tau} = a \exp(-bq) - L \quad (9b)$$

where  $t$  and  $\tau$  represent two separate time frames.

Using the fourth assumption, these rate equations can now be converted to forms describing the chemisorption-photoconduction process in terms of the time-variable density,  $n \equiv n(t)$ , of conduction electrons. Let  $n_s$  be the value of  $n$  for photocurrent saturation, and  $q_s$  the corresponding value of  $q$ . Consider the general case in which the photocurrent does not reach saturation, but attains a maximum such that the maximum value of  $n$  is  $n_f = fn_s$ ,  $f \leq 1$ . Let  $q_f$  be the corresponding value of  $q$ . If  $V$  is the volume of the solid under consideration and  $\alpha$  is the area illuminated, then

$$\Delta N = V\Delta n = V(n_f - n) \text{ and } \Delta Q = \alpha\Delta q = \alpha(q - q_f).$$

It follows from the fourth assumption that

$$q - q_f = V\Delta n/\alpha$$

or

$$q = x_0\Delta n + q_f \quad (10)$$

where  $x_0 = V/\alpha$  is a constant geometrical factor.

Differentiating Equation 10 gives

$$\frac{dq}{dt} = x_0 \frac{d(\Delta n)}{dt}$$

and substitution of the expression for  $q$  in Equation 10 into the right side of Equation 9a (the decay equation) gives

$$a \exp(-bq) = a \exp(-bx_0\Delta n - bq_f).$$

With these changes Equation 9a becomes

$$\frac{d(\Delta n)}{dt} = A \exp(-B\Delta n) \quad (11)$$

where  $A = ax_0^{-1} \exp(-bq_f)$  and  $B = bx_0$ .

But  $A$  is a function of  $n$ , since  $a = a'(P,T)n$ . Let  $A' = a'(P,T)x_0^{-1} \exp(-bq_f)$ .

Then

$$\frac{d(\Delta n)}{dt} = A'n \exp(-B\Delta n) \quad (12)$$

where  $\Delta n \equiv \Delta n(t) = n_f - n(t)$ . Let  $y = \Delta n/n_f$ . Then Equation 12 becomes

$$\frac{dy}{dt} = A'(1-y)\exp(-\beta y) \quad (13)$$

where  $\beta = Bn_f$ . Rearranged for integration, Equation 13 becomes

$$\int_0^y \frac{e^{\beta y} dy}{1-y} = \int_0^t A' dt = A't \quad (14)$$

For  $y < 1$ ,  $1/(1-y) = 1 + y + y^2 + \dots$  and  $\int_0^y \frac{e^{\beta y} dy}{1-y} =$   
 $\int_0^y (1 + y + y^2 + \dots) \sum_{p=0}^{\infty} \frac{(\beta y)^p}{p!} dy = \frac{1}{\beta} \sum_{p=0}^{\infty} \frac{(\beta y)^{p+1}}{(p+1)!} + \frac{1}{\beta^2} \sum_{p=0}^{\infty} \frac{(\beta y)^{p+2}}{(p+2)p!}$

plus terms of higher order. Using only the first term of this expansion, Equation 14 becomes

$$A't = \frac{1}{\beta}(e^{\beta y} - 1)$$

or

$$e^{\beta y} = \beta A't + 1 \quad (15)$$

Taking logarithms of both sides and dividing by  $\beta$  gives

$$y = \frac{1}{\beta} \ln(\beta A't + 1) \quad (16)$$

The constant  $\beta A'$  has dimensions of reciprocal time, so set  $\beta A' = t_d^{-1}$ .

With this substitution and using  $\beta = Bn_f$  and  $y = \Delta n/n_f$ , Equation 16 reduces to

$$\Delta n = \frac{1}{B} \ln\left(\frac{t}{t_d} + 1\right) \quad (17)$$

where  $t_d^{-1} = Bn_f A'$ . This expression constitutes a first-order approximation to a solution for Equation 11, and is restricted to cases in which  $\Delta n/n_f$  is small. If  $\Delta n/n_f$  becomes so large that higher order terms in  $y$  can no longer be neglected, then Equation 17 takes the form

$$\Delta n(t) = \frac{1}{B} \ln\left[\frac{t+t_d}{t_d} - \sum_{m=2}^{\infty} \sum_{p=0}^{\infty} \frac{(\beta y)^{p+m}}{\beta^m (p+m)p!}\right] \quad (18)$$

in which the summation is positive, since  $0 < y < 1$  and  $\beta = e^2 n_i x_o / C_a kT > 0$ .

Equation 11, being the rate equation applicable to cases in which there is no desorption due to incident illumination, can be used to describe the photocurrent decay following a period of illumination in which the conduction electron density has reached a maximum value  $n_i$ . For cases in which  $y$  is small,  $\Delta n(t) = n_i - n(t)$  should increase linearly with  $\ln(t + t_d)$ . However, should the higher order terms represented by the summation in Equation 18 become appreciable, then a plot of  $\Delta n(t)$  vs  $\ln(t + t_d)$  should be expected to show a sublinear behavior,  $\Delta n(t)$  varying as a power of the logarithmic term that is somewhat less than unity.

Now consider the case in which the photodesorption term  $L$  enters into the rate equation. The appropriate equation is then

$$\frac{dq}{d\tau} = a \exp(-bq) - L \quad (9b)$$

where illumination begins at time  $\tau = 0$ . If  $n_e$  is the equilibrium conduction electron density in the dark and  $q_e$  is the corresponding chemisorbate density, then

$$\alpha(q_e - q) = V(n - n_e) = V\Delta n_e$$

or

$$q = -x_o \Delta n_e + q_e \quad (19)$$

Note that  $\Delta n_e \equiv \Delta n_e(t)$  is not the  $\Delta n(t)$  defined for the decay process.

Now

$$\frac{dq}{d\tau} = -x_o \frac{d(\Delta n_e)}{d\tau} \quad (20)$$

and

$$\exp(-bq) = \exp(bx_o \Delta n_e - bq_e) \quad (21)$$



Substituting Equations 20 and 21 into Equation 9b (the rise equation) gives

$$\frac{d(\Delta n_e)}{d\tau} = x_0^{-1} \left[ L - A_1 \exp(B\Delta n_e) \right] \quad (22)$$

where  $B = bx_0$ , as before, and  $A_1 = a \exp(-bq_0)$ . Rewriting and integrating, Equation 22 becomes

$$\int_0^{\Delta n_e} \frac{d(\Delta n_e)}{L - A_1 \exp(B\Delta n_e)} = \int_0^{\tau} \frac{d\tau}{x_0} = x_0^{-1} \tau \quad (23)$$

or, if the photodesorption rate  $L$  is assumed constant,

$$\frac{\Delta n_e}{L} - (BL)^{-1} \left\{ \ln[L - A_1 \exp(B\Delta n_e)] + \ln(L - A_1) \right\} = \tau/x_0.$$

Rearranging and multiplying by  $BL$ , this becomes

$$B\Delta n_e = \ln \left[ \frac{L - A_1 \exp(B\Delta n_e)}{L - A_1} \right] + BL\tau/x_0.$$

Taking the antilogarithm of both sides and substituting  $b$  for  $B/x_0$  gives

$$\exp(B\Delta n_e) = \left[ \frac{L - A_1 \exp(B\Delta n_e)}{L - A_1} \right] \exp(bL\tau).$$

Regrouping and simplifying, this becomes

$$\exp(B\Delta n_e) = \left[ \frac{A_1}{L} + \left(1 - \frac{A_1}{L}\right) \exp(-bL\tau) \right]^{-1}.$$

Taking logarithms of both sides and dividing by  $B$  now gives

$$\Delta n_e(\tau) = -\frac{1}{B} \ln \left[ \frac{A_1}{L} + \left(1 - \frac{A_1}{L}\right) \exp(-bL\tau) \right] \quad (24)$$

This solution, like the solution for the decay equation, is an approximation since  $A_1$  is a function of  $n$ . Note that there is no simple relationship between  $\Delta n_e(\tau)$  and  $\tau$ , unless  $L \gg A_1$ , in which case  $\Delta n_e(\tau)$  should approximate a linear function of  $\tau$ . Also note that if  $\tau$  becomes very large (photocurrent saturates)  $\Delta n_e$  approaches the constant  $(\Delta n_e)_{sat} = B^{-1} \ln(L/A_1)$ .

One is to be reminded that the validity of this model for the surface-related photoconductivity of sintered zinc oxide has been

investigated by Medved (16) and that its applicability to the case of the surface-sensitive photoconductivity in stannic oxide crystals forms a major area of consideration in the experimental work described in the following chapters.

## CHAPTER III

### SAMPLES, APPARATUS, AND EXPERIMENTAL METHODS

#### Natural Samples

The samples used for the major part of this investigation were rectangular slabs cut from natural cassiterite obtained from Araca, Bolivia. These slabs were of two thicknesses, near one millimeter and near one-half millimeter, and had other dimensions ranging up to more than ten millimeters. These samples were cut with a diamond saw from regions of the natural crystals selected for optical transparency, lack of color, and scarcity of visible mechanical defects. The broad faces of these slabs were polished by successive lappings with No. 320 SiC paper, Centriforce abrasive M304, and Linde "A" polishing compound.

None of the samples thus prepared was entirely free of flaws, the most nearly perfect specimens having a few internal cracks of microscopic size. Several of the less select samples contained prominent fractures, and only a few were without some coloration. All samples were transparent, but several exhibited a nearly uniform yellow to yellow-green tinge, while others had localized dark brown to black regions.

These colorations indicated the presence of impurities. A spectroscopic analysis\* of scrap sample material showed silicon,

---

\*Analysis by The Bruce Williams Laboratories, Joplin, Missouri.

aluminum, and iron to be present, along with lesser amounts of magnesium, titanium, lead, and copper. Estimated maximum percentages ranged from 0.05 to 0.5 per cent for silicon, the most abundant impurity.

In general, there was considerable inhomogeneity of color and electrical conductivity in the natural crystals from which the samples were cut. The use of relatively small samples minimized the undesirable effects that such inhomogeneities might produce in the various measurements of physical properties. Point contact checks showed that areas of low surface resistivity were scattered randomly over the polished and unpolished faces of all samples studied.

The electrical conductivity of these samples has been found to be n-type and ranges in magnitude from  $10^{-6}$  ohm<sup>-1</sup> - cm<sup>-1</sup> to  $10^1$  ohm<sup>-1</sup> - cm<sup>-1</sup>. Typical room temperature values for colorless or slightly yellowish samples were noted to fall in the range between  $10^{-4}$  ohm<sup>-1</sup> - cm<sup>-1</sup> and  $10^{-3}$  ohm<sup>-1</sup> - cm<sup>-1</sup>. Point contact checks have revealed that brown or black areas, which are often opaque, have a very high conductivity. The work of Tolly (26) has indicated that impurity band conduction may occur in these samples, with a donor level approximately 0.7 eV below the conduction band. Data obtained for a limited number of samples indicates that the Hall mobility varies as  $T^{-1.3}$  at high temperatures, the variation persisting to lower temperatures for samples of higher conductivity. (26).

The basic features of the photoconductivity of these samples have been studied by Hurt (27). A DC photoresponse characterized by slow rise and decay and a photocurrent saturation after one to three hours' continuous exposure was found in all samples having a dark

conductivity not greatly exceeding  $10^{+3}$  ohm<sup>-1</sup> - cm<sup>-1</sup>. In addition to the slow effect, a much less pronounced fast effect was revealed in AC measurements on the same samples, suggesting that two separate sets of recombination levels exist.

The natural samples used in the major part of the present study are briefly described in Table I. All have a short wavelength optical cutoff near 360 mμ and all show photoconductivity. Sample II is somewhat peculiar in its photoconductive behavior as well as in its low dark conductivity. The photoresponse of this sample is considerably more sensitive than that of any other sample, and the photocurrent has never been seen to reach a saturation. Samples IV and VIII have dark brown to black regions at one end, and lesser reddish-brown to dark brown spots can be seen in Samples III, VI, and XVII.

#### Artificial Samples

Less extensive work has been carried out on small artificial samples grown in this laboratory. These were in the form of needles having a rectangular cross section, the largest being roughly 0.1 mm x 0.1 mm x 4.0 mm. The ones chosen for investigation of electrical properties are colorless single crystals having no visible imperfections other than smooth microscopic growth patterns on the surfaces. These were used in their original state in most cases, being subjected to no treatment other than the usual cleaning procedure described in the next section.

The work carried out on the artificial samples consisted of measurements of photoresponse at several temperature points and in oxygen-rich and oxygen-free ambients. Also, the variation of

photoresponse with wavelength of the incident light was measured in several artificial samples, and rough measurements of their dark conductivity were carried out. The effects of surface treatment were also briefly examined.

TABLE I

## APPEARANCE AND DARK CONDUCTIVITY OF NATURAL SAMPLES

Sample	Dimensions (mm <sup>3</sup> )	Appearance	Dark Conductivity (ohm <sup>-1</sup> - cm <sup>-1</sup> )
II	6.2 x 2.2 x 1.5	Colorless	$6.3 \times 10^{-7}$
III	5.7 x 3.2 x 0.95	Colorless	$5.6 \times 10^{-5}$
IV	8.3 x 5.0 x 0.91	Clear, faintly yellow-green	$2.3 \times 10^{-4}$
VI	5.7 x 4.7 x 1.00	Colorless	$6.4 \times 10^{-5}$
VIII	10.7 x 6.1 x 1.01	Colorless	$1.1 \times 10^{-4}$
XIIIA	6.0 x 2.7 x 0.58	Colorless	$2.8 \times 10^{-4}$
XVII	11.0 x 3.6 x 0.56	Colorless	$2.6 \times 10^{-4}$

## Sample Cleaning and Contact Materials

In order to minimize the likelihood of obtaining erroneous results due to foreign material attached to the surface of a sample, each sample was cleaned as follows before mounting in a sample holder. The first step was a bath in aqua regia (75% HCl, 25% HNO<sub>3</sub>), followed by a distilled water rinse and successive immersions in acetone and methyl alcohol. The acetone and alcohol washes were each usually of two to three hours' duration, while the bath in aqua regia was often twelve hours or longer.

Nearly all mounting was done with silver paint (DuPont 4817) used as the contact adhesive. Indium or an indium amalgam served as the contact material in a limited number of cases, but while indium is capable of wetting the stannic oxide surface, the surfaces of these natural samples would be wetted only at scattered locations. Indium was never seen to provide any advantage in the electrical performance of contacts.

Following the removal of a sample from its holder, the sample was washed in acetone to remove any silver paint that might remain on the surface.

#### Apparatus for Effect of Ambient on Photoconductivity

Of central importance to this and several of the other phases of this work was the vacuum system, a block diagram of which is shown in Figure 2. Except for the forepump, a Cenco "Hyvac 7," and lines to the water jackets on the diffusion pump, the system was constructed of glass. The diffusion pump was of a four stage design capable of maintaining pressures below  $1 \times 10^{-7}$  millimeters of mercury, with Dow Corning 703, a silicone oil, being the pump fluid used.

Three pressure gauges with overlapping ranges provided for measurement of system pressures from atmospheric pressure to  $1 \times 10^{-7}$  millimeters of mercury. In order of decreasing ranges, these were a mercury column, a McLeod gauge, and a Miller Laboratories Model 100-A cold cathode ionization gauge.

Individual sample holders were removable, being joined to system manifolds by means of ball and socket ground glass joints. A stopcock was built into each side outlet, and all separable joints were sealed

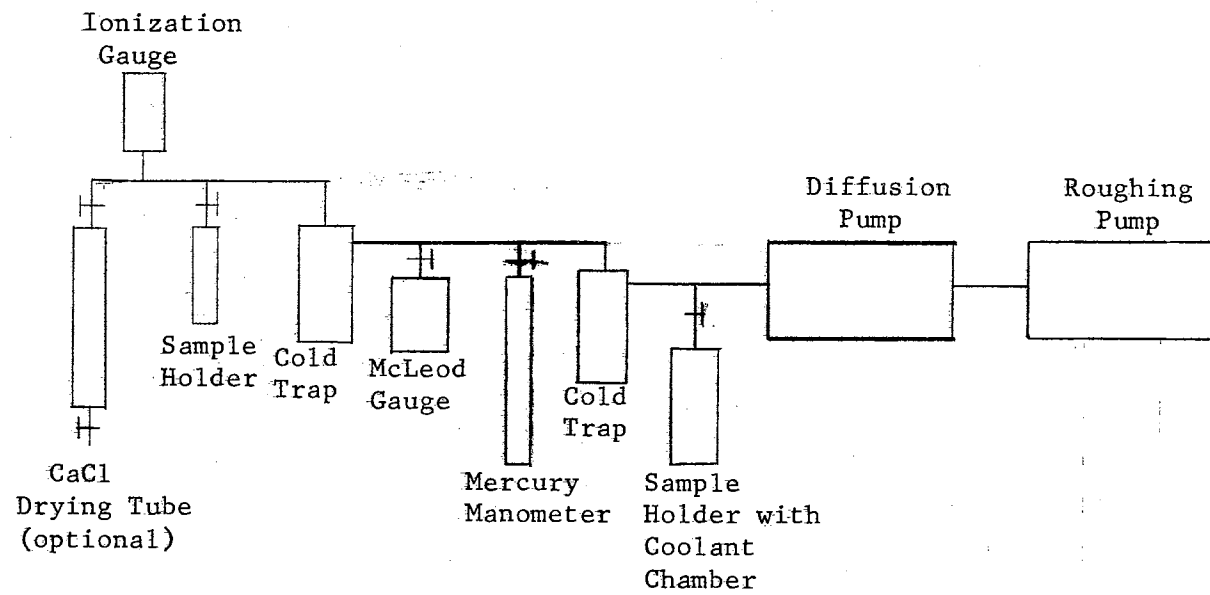


Figure 2. Block Diagram of Vacuum System



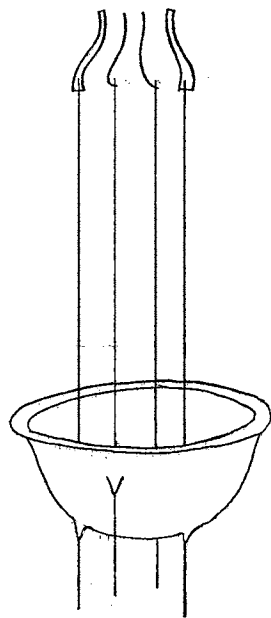
with Apiezon "T" grease, stopcocks with Apiezon "N" grease. Also included in the system were two liquid nitrogen cold traps.

The sample holder used in most of the room temperature studies consisted of the two glass pieces shown in Figure 3. The four electrodes were silver soldered onto tungsten wires which were sealed into the glass wall of the lower piece and provided for external attachment of a power supply and measuring instruments. Two electrodes were flexible copper strips which could be sprung to separations capable of accommodating most of the available samples. These served as end contacts. The other two electrodes were short lengths of 30 gauge (B & S) copper wire which could be attached to the side of a sample for use as potential probes. The remaining glass piece, which served to join the base described above (built on a No. 35 socket) to the manifold (equipped with No. 18 joints), had a central portion of vycor tubing which admitted light of the near ultraviolet wavelengths to the sample.

#### Measurement of Ambient Effect on Photoconductivity

Two general approaches were employed in the determination of the relative importances of various gaseous ambients in the photoconductive behavior of stannic oxide. One was based on a series of separate experiments in which the ambient was changed between experiments, all other factors held constant, and the sets of data obtained compared. The other involved single experiments conducted in the same general manner, but with the change of ambient brought about during the course of an experiment. The former method, which was the more frequently used, will be described first. Only room temperature work will be

Tungsten Wires  
with Electrodes



1" O.D.  
Vycor  
Tubing

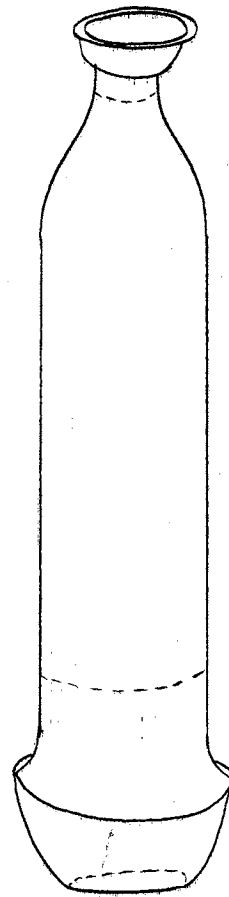


Figure 3. High Vacuum Sample Holder.

discussed in this section.

It was necessary in a series of experiments, each with a specific ambient held at a constant pressure, to ensure that illumination, temperature, and contacts were not altered at any time during the series. Illumination was the most critical factor, inasmuch as a change of either the intensity or the portion of the sample under direct illumination could produce data that might easily be misinterpreted as arising from differences due to a change of ambient. For this reason considerable care was taken in establishing a light source-sample geometry at the beginning of a series of experiments and in checking this geometry throughout the series. The light source used was a mercury arc lamp, the full spectrum being employed. Changes in the contacts, which were of silver paint, in these room temperature experiments did not occur without mechanical disturbance of the sample holder, which at the same time altered the geometry and with it the illumination. Fluctuations in temperature posed no problem, room temperature being reliably maintained between 295°K and 298°K by the air conditioning system.

The time factor was also of considerable importance in these experiments, as direct current was used throughout. In a given series of experiments it was necessary for all periods of illumination to be the same, and ample time had to be allowed for complete decay of photocurrent following each excitation. This latter period ranged from five to twenty hours, being dependent upon sample, ambient, and illumination.

Ambients used in these series of experiments included air, oxygen, nitrogen, helium, and vacua having pressures down to  $5 \times 10^{-8}$

millimeters of mercury. When being filled with a gas other than air, the system was swept for several minutes before being closed with the gas to be used in order to minimize partial pressures of residual foreign gases. A calcium chloride drying tube was attached to the system input so that the water vapor content of the incoming gas could be reduced if desired. Provision was also made for bubbling the incoming gas through water to increase its water vapor content. The second method, in which was used the same apparatus as in the procedure described above, was highly useful in comparing the effects of two ambients, but by its nature was limited to no more than two in any one experiment. The change of ambient could occur during either the rise or decay of photocurrent. The procedure most often used, however, was to maintain a vacuum throughout the period of illumination and during the initial part of the photocurrent decay, then allow the gas in question to flow into the system, at which time a change in the rate of decay might be expected to occur.

Data were obtained in two ways in connection with the procedures described in this section. The four-electrode sample holder enabled measurement of the actual bulk conductivity of the illuminated portion of the sample during and following the exposure. A Leeds and Northrup Type K-3 potentiometer was used for measurement of the potential drop between the two central probes, while a Sensitive Research Instruments DC microammeter was usually employed in monitoring the current. Current values were often so small as to require such a meter in preference to a ten ohm standard resistance used in connection with the potentiometer because of its better resolution in the 0.01-0.50  $\mu\text{a}$  range.

The potential probes, like the end contacts, were attached to the sample with silver paint. For conductivity calculations the distance between these electrodes was measured with a traveling microscope. Other relevant sample dimensions were determined by means of a micrometer caliper.

In these four-electrode measurements the vycor sample holder was covered so that the only part of the sample illuminated was that portion between the two central probes.

The outstanding disadvantage of this method was the comparatively slow point-by-point acquisition of data, with periods of thirty seconds or more elapsing between adjacent data points. While capable of furnishing highly accurate data in extended rises and decays of photoconductivity, this method was somewhat unsatisfactory at times when the conductivity was changing rapidly, as at the beginning of an exposure or during the initial seconds of a decay.

By sacrificing some precision, continuous rise and decay curves could be obtained. The method used was the obtaining of a recorder trace of the photocurrent with only the two end electrodes attached to the sample. A bucking voltage was applied to the input of the DC amplifier to cancel the dark current and leave only the photocurrent to be amplified and recorded. The DC amplifier used was a General Electric Model 8901490G2 self-balancing potentiometer and the recorder a Texas Instruments "Recti-riter." Knowledge of circuit parameters enabled the data thus obtained to be rewritten in terms of relative conductivities.

### Apparatus for Effect of Temperature on Photoconductivity

For measurements of photoconductivity at temperatures other than room temperature a special sample holder was designed for use with the vacuum system and electrical instrumentation described earlier. In order to permit simultaneous measurements of the influences of ambient and temperature, the sample holder was constructed so that the sample could be mounted in a chamber with a direct outlet to the vacuum system and be in good thermal contact with a refrigerant in a separate chamber. An exploded sectional view is shown in Figure 4.

The vacuum chamber was a rectangular stainless steel box fitted with a circular opening and flange of such dimensions as to accommodate the cylindrical brass coolant chamber. These two pieces were joined with Allen screws, a neoprene O-ring and Apiezon "N" grease providing an airtight seal. The sample was clamped between the bottom of the coolant chamber and a circular platform supported by screws fitting tapped holes in the bottom of the coolant chamber.

The coolant chamber was the electrical ground. The electrode of opposite polarity was a brass cylinder having a diameter of nearly seven millimeters and a height of two millimeters. Soldered into this small cylinder were one of the leads to the crystal and a copper-constantan thermocouple junction. Connections with external leads were made through ceramic pass-throughs silver soldered into the upper wall of the stainless steel chamber. Insulation of this cylinder from the supporting platform was achieved through the use of two short lengths of glass tubing, one serving as a base, the other as a sleeve. These slipped into a hole drilled in the center of the platform.

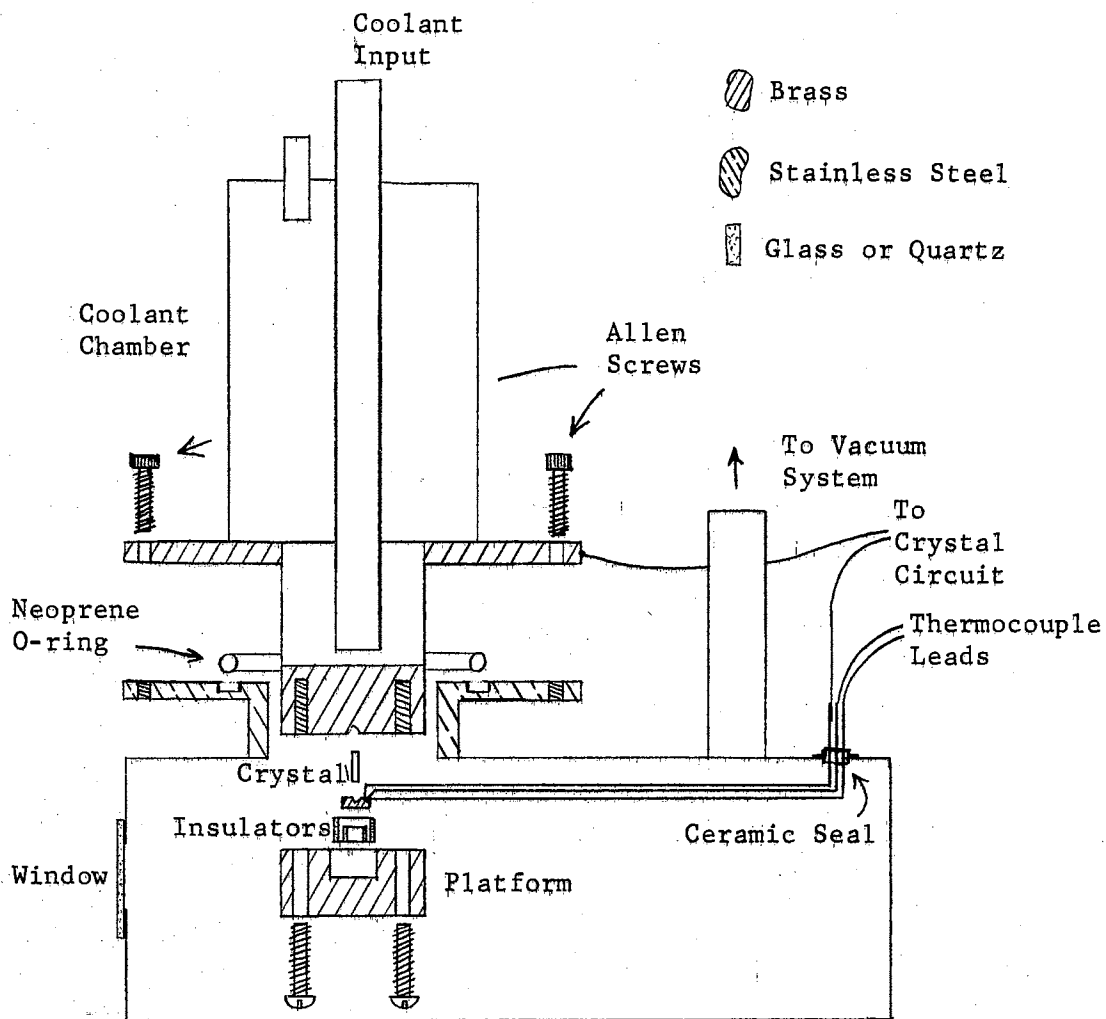


Figure 4. Low Temperature Sample Holder.



This, along with grooves in the cylinder and the bottom of the coolant chamber, provided a rigid mounting for samples, the grooves being aligned so that a broad face of a natural sample faced the circular window in the front of the sample holder. The window was a polished quartz plate one millimeter thick attached to the stainless steel by Fisher's "Sealit."

This design permitted measurements of only the two-contact type. Contact materials used were indium amalgam and silver paint, more often the latter because of its superior mechanical behavior over the temperature range between  $80^{\circ}\text{K}$  and  $375^{\circ}\text{K}$ .

The coolant chamber was equipped with an input tube extending nearly to the floor of the chamber. A second tube was set in the upper wall to provide an escape for gases. A nichrome heating coil was constructed so as to fit into the input tube.

#### Measurement of Temperature Effect on Photoconductivity

As in most room temperature measurements of the ambient effect on photoconductivity, measurements of the temperature effect were conducted as a series of separate experiments in which all factors except temperature and ambient were held constant from experiment to experiment. In a single experiment, both temperature and ambient were not changed unless it was required to measure the effect of change of ambient at a particular temperature, in which case the procedure described in a previous section was used. Because of the use of DC measuring methods it was not possible to obtain any useful data by analogous variations of temperature since, of course, relative temperature changes could be achieved much less rapidly than pressure changes.



It was necessary to maintain a constant illumination throughout a series of experiments and to make direct comparisons only between experiments of like periods of illumination.

The temperature range covered in measurements using the sample holder described in the preceding section was between 81°K and 373°K. The fluids used for temperature adjustment were, in order of increasing temperature, liquid nitrogen, acetone with dry ice, methanol under rough vacuum, water under rough vacuum, water with heating coil, and paraffin oil with heating coil.

#### Measurement of Ambient Effect on Dark Conductivity

The four-electrode vacuum sample holder described above and the K-3 potentiometer were used for these measurements, employing the same technique as was used to measure the effect of ambients on photoconductivity. It was necessary in these measurements to be sure the sample had been shielded from illumination, particularly ultraviolet, for a length of time sufficient to allow complete decay of photoconductivity. In any one set of measurements, several readings would be taken in the first ambient. Then the system would be swept with the second ambient, or an inert gas, before again closing the system with the second ambient surrounding the sample. A second series of readings would be taken in the same manner as with the first ambient, and these readings would then be compared with those obtained with the first ambient. The effects of any number of ambients could be compared in this manner. These were room temperature measurements.

### Contact Potential Measurements

To measure the effect of change of ambient on the height of the surface barrier, a small Kelvin apparatus was constructed and housed in a bell jar with a connection to the vacuum system. The Kelvin method of contact potential measurement consists of determining the DC potential required to null the AC signal generated by periodically varying the separation of two plates of a parallel plate capacitor, one of which consists of a reference material and the other of the material being investigated. The broad face of a natural stannic oxide sample was the stationary plate and a rectangle of platinum foil was the driven plate, a frequency of 40 cps being used. The DC potential measured is equal and opposite to the difference between the barrier heights of the two electrodes.

The separation between the two plates was roughly 0.5 mm and the amplitude of vibration 0.1 to 0.2 mm. The AC detector was a basic electrometer circuit using a Victoreen 5800 electrometer tube. The output of this impedance-matching stage was fed to an AC millivoltmeter (Hewlett-Packard 400D) which was used as the null detector. This system was sufficiently sensitive to detect changes of less than 0.010 volts.

All measurements were obtained in the dark at room temperature, and continuous monitoring during change of ambient was possible. The DC voltage required to maintain an AC null was recorded frequently before, during, and after each change of ambient.

### Oxidation and Reduction

Three natural samples, VI, VIIIA, and VIIIB, were heated to approximately 925°K in various atmospheres in attempts to produce

measurable alterations in their electrical and/or optical properties. Sample VI was heated in one atmosphere of oxygen, sample VIIIA in one atmosphere of hydrogen, and sample VIIIB in a vacuum of about  $10^{-3}$  mm of mercury. Time of heating was 15 minutes in each case, except for the second heating of sample VIIIA in hydrogen, which was of 150 minutes' duration. A small tube furnace with a resistive heating element was used, the sample being placed on three needle points of a stainless steel holder in a vycor tube. Two tubes, both of vycor, were used. The tube used in the vacuum reduction was sealed at one end and attached to the vacuum pump, while the other, used in the oxygen and hydrogen runs, was open at both ends to permit continuous gas flow. In each case the atmosphere in which the heating took place was maintained until the sample and holder had cooled to room temperature. Following each period of heating, the sample used was left in aqua regia for at least one day to remove any surface deposits and to allow any effects of a temporary nature to subside or to reveal their presence by a partial subsidence.

#### Wavelength Dependence of Photoconductivity

Using a Bausch and Lomb monochromator and mercury arc light source, the relative responses at several wavelengths in the ultraviolet region were measured in several artificial samples. An electric drive on the monochromator permitted the region of interest to be scanned while photocurrent was recorded using the system described earlier in this chapter. At each wavelength the peak photocurrent was assumed to be proportional to the number of photocurrent carriers generated. Assuming the same proportionality to exist at all wavelengths at which data were

obtained, the relative responses could be calculated. The relative intensities of the mercury lines as seen by a sample at the exit slit of the monochromator were measured by a Charles M. Reeder & Company thermopile placed in the sample mounting position and used in conjunction with a Leeds and Northrup Type K-3 potentiometer. With this calibration the relative response per unit intensity and relative quantum efficiencies could be calculated.

Similar measurements were made on a few of the natural samples, but the results obtained were such as to permit only a rough qualitative interpretation.

#### Other Experimental Work

Samples II and XXIIB were heated in vacuum to a temperature exceeding  $1200^{\circ}\text{K}$  while in contact with indium metal to determine what effects the diffusion of a trivalent impurity into stannic oxide might produce. Measurements of dark conductivity and photoconductivity in air at room temperature were made before and after the indium diffusion took place. This work was of an exploratory nature, being an attempt to assign a cause to certain anomalous behavior noted in sample II.

In order to determine relative magnitudes of surface and bulk electrical conductivity, the variation of resistance with location and area of painted contacts was measured in the dark at room temperature in natural samples VI, XIII A, XVIII, and XXIII. This enabled a rough estimate of the ratio of surface to bulk conductivity to be made.

In connection with the low temperature photoconductivity work, a number of attempts to measure thermally stimulated current arising from shallow trapping levels were made. The current rise during warming

was recorded following the recording of photocurrent decay at low temperature, using the same instrumentation.

## CHAPTER IV

### RESULTS

#### Introductory Statements

In this chapter the results of the work described in the preceding chapter will be presented, following a section outlining the method of data reduction employed for the major part of the work. A discussion of their importance will be deferred to the following chapter.

#### Initial Photoconductivity Calculations

The quantity sought in both types of photoconductivity measurement outlined in the previous chapter was the time variation of conductivity during illumination and during the period of decay, the latter being of greater interest. This was measured in a more nearly direct manner by the four-contact method, the voltage  $V$  across the illuminated area and the current  $i$  through the sample both being determined as a function of time. The conductivity  $\sigma(t)$  at time  $t$  was calculated using the formula

$$\sigma(t) = \frac{i(t)l}{V(t)A} \quad (25)$$

where the probe separation  $l$  and the cross sectional area of the crystal were constants. Determination of the dark conductivity  $\sigma_0$  and the conductivity  $\sigma_{max}$  at the instant illumination ceased (photo-current not necessarily saturated) permitted calculation of the ratio of the time-varying conductivity to the dark conductivity during rise,

$\sigma(t)/\sigma_0$ , and the fractional change during decay, defined as  $[\sigma_{\max} - \sigma(t)]/[\sigma_{\max} - \sigma_0]$ . These conductivity values are bulk averages for the portion of the crystal available for direct illumination.

In the two-contact method, the quantity measured directly was the photocurrent. Dark current, applied voltage, and series resistances were measured independently in order to calculate actual relative conductivity changes of the crystal as a function of time. With the chart speeds available for recording the photocurrent, data point separations as small as 0.5 sec were obtainable. In these measurements the crystal was illuminated from end contact to end contact, routine checks having shown that illumination of contact boundaries had no noticeable effect on the rise and decay of photocurrent.

Letting  $V$  represent the applied voltage,  $R_s$  the total resistance in series with the crystal, and  $i'(t)$  the total current at time  $t$ , the current  $i(t)$  which would flow through the crystal with the same applied voltage and no series resistance was calculated using the formula

$$i(t) = V \left[ \frac{V}{i'(t)} - R_s \right]^{-1} \quad (26)$$

Knowledge of the corresponding dark current  $i_0$  and total current  $i_{\max}$  at the instant illumination ceased allowed analysis of rise curves in terms of the quantity  $i(t)/i_0$  and of decay curves in terms of  $[i_{\max} - i(t)]/[i_{\max} - i_0]$ . Since the geometrical and voltage factors cancel, and it has been assumed that there is no change of mobility involved in the light-induced conductivity changes

$$\frac{i(t)}{i_0} = \frac{\sigma(t)}{\sigma_0} = \frac{n(t)}{n_0} \quad (27a)$$

and

$$\frac{i_{\max} - i(t)}{i_{\max} - i_0} = \frac{\sigma_{\max} - \sigma(t)}{\sigma_{\max} - \sigma_0} = \frac{n_f - n(t)}{n_f - n_0} \quad (27b)$$

Although contact resistance has not been considered, the above implied constancy of applied voltage across the samples is not invalidated in view of the small current changes which were treated. The reasons for choosing expressions of the above forms will be discussed in the next section.

#### Effect of Ambient on Photoconductivity

The basic features of the photoconductivity exhibited by the natural samples were not greatly affected by the composition of the surrounding gaseous ambient. All natural samples in which photoconductivity could be detected continued to respond to ultraviolet radiation in all ambients tried, with the slow rise and decay dominant in all cases. However, there was a definite dependence of the over-all sensitivity of any particular sample on the ambient's composition, and this dependence was found to be generally the same in all samples in which the effect was measured. Any ambient having in its makeup an appreciable percentage of oxygen was found to reduce the sensitivity of a natural sample and to hasten photocurrent decay in such a sample. The form of the oxygen used in all work was the ordinary diatomic variety.

In Figure 5 are shown two short-period rise curves obtained under identical conditions except for the pressure of the ambient. These curves, which illustrate the effect of oxygen on the photocurrent rise in sample IV, are representative of the short-exposure rise curves obtained for this sample and the other natural samples upon which such work was done. The quantity plotted is the ratio of total current to the dark current, with time the abscissa. This ratio, by Equation 27a, is equal to the conductivity ratio and the carrier density ratio. Hall



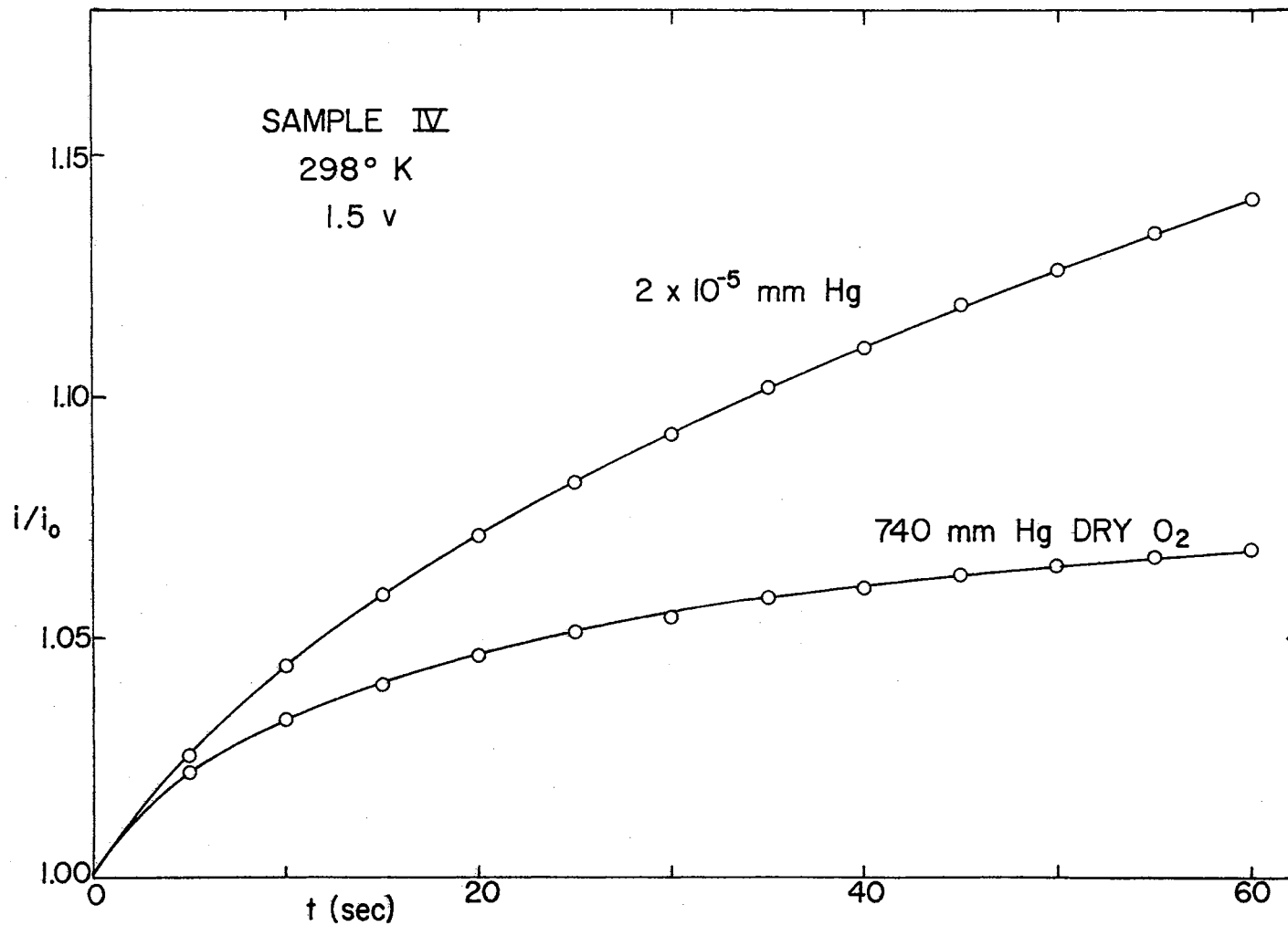


Figure 5. Typical Photocurrent Rise Curves for a Natural Sample

measurements have revealed that the carrier density in sample IV in the dark at room temperature is slightly less than  $1 \times 10^{14} \text{ cm}^{-3}$ .

Figure 6 shows the decay curves which followed the one-minute exposures that produced the rise curves of Figure 5. In this case the quantity plotted is the ratio of Equation 27b, which represents the fraction of the photoconductivity having decayed, time again being the abscissa. Figure 7 shows the same two decay curves, but with the logarithm of time as the abscissa. Again, these are representative of the decays observed in several natural samples.

The type of result obtained by changing the ambient during the course of a single experiment is illustrated in Figures 8, 9, 10, and 11. Figure 8 shows the effect of evacuating the sample holder--initially containing air at atmospheric pressure--during the photocurrent rise. The withdrawal of the oxygen-rich ambient enables the photoconductivity to build to a level well above what it would have been had the air been left in the sample holder. The dependence on the ambient is noticeably greater in sample XIII A than in sample IV.

Figure 9 illustrates the effect of admitting an oxygen-rich ambient to the sample while the photocurrent decay is in progress. The photocurrent rise and the initial part of the decay had taken place in vacuum. The decay shown followed an exposure of three minutes duration.

A similar result is shown in Figure 10. Unlike the results shown in Figures 5 through 9, which were taken from recorder traces of the photocurrent and involved time periods of no more than three minutes, this curve represents data obtained using four-contact potentiometric conductivity measurements taken over a considerably longer time interval. As in Figure 9, the fraction of photocurrent remaining, rather than the

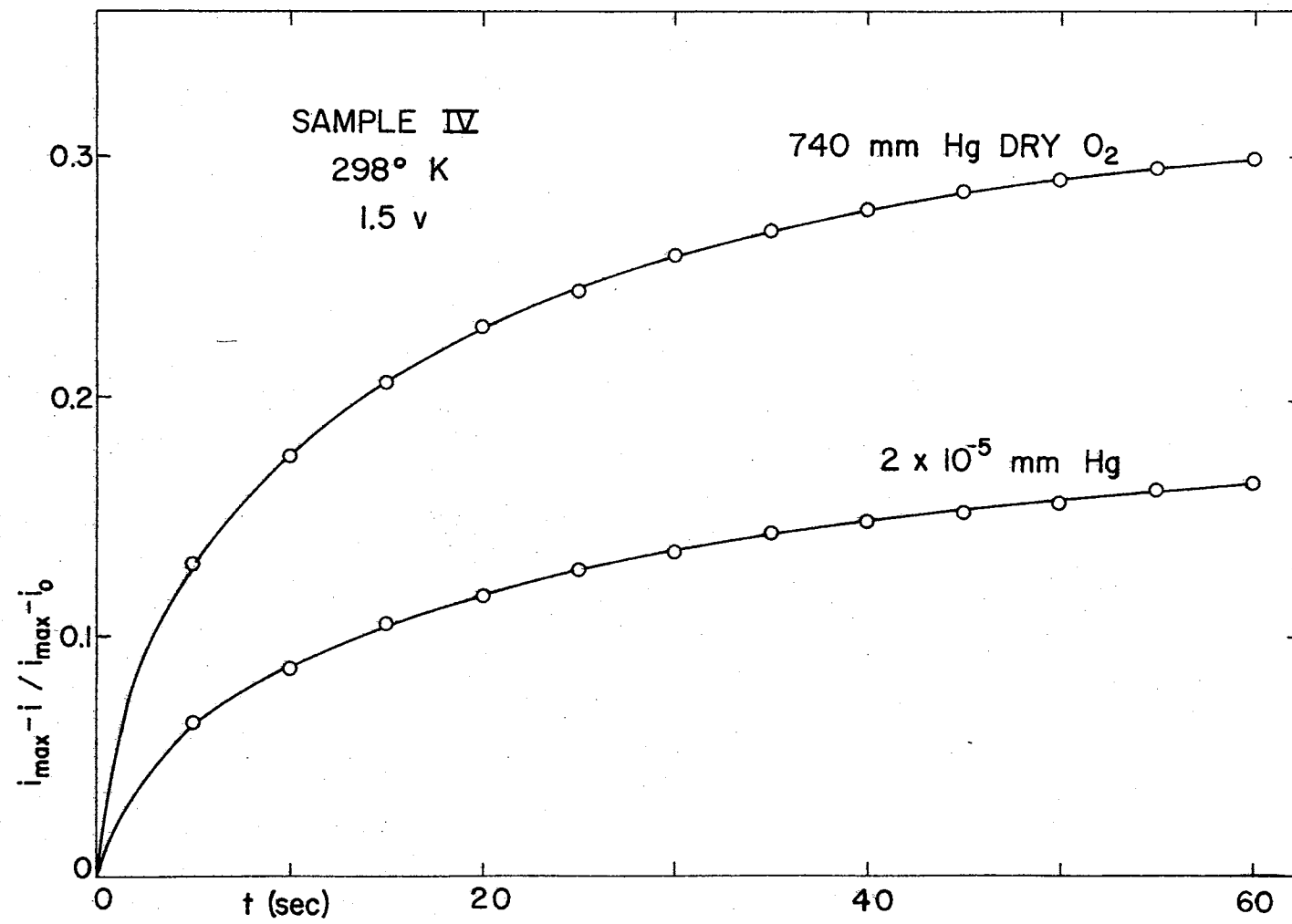


Figure 6. Typical Photocurrent Decay Curves for a Natural Sample

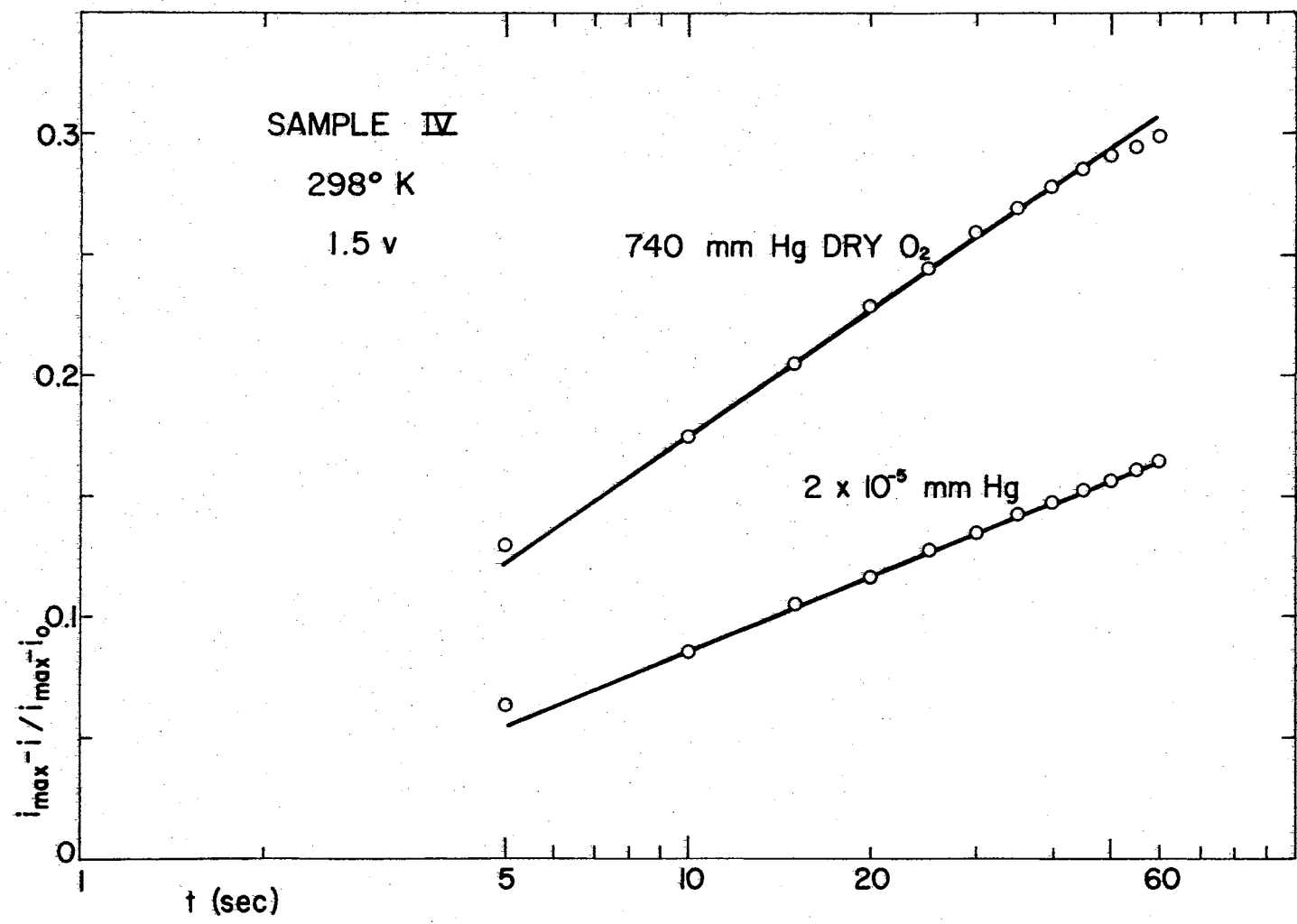


Figure 7. Logarithmic Decay Curves for a Natural Sample

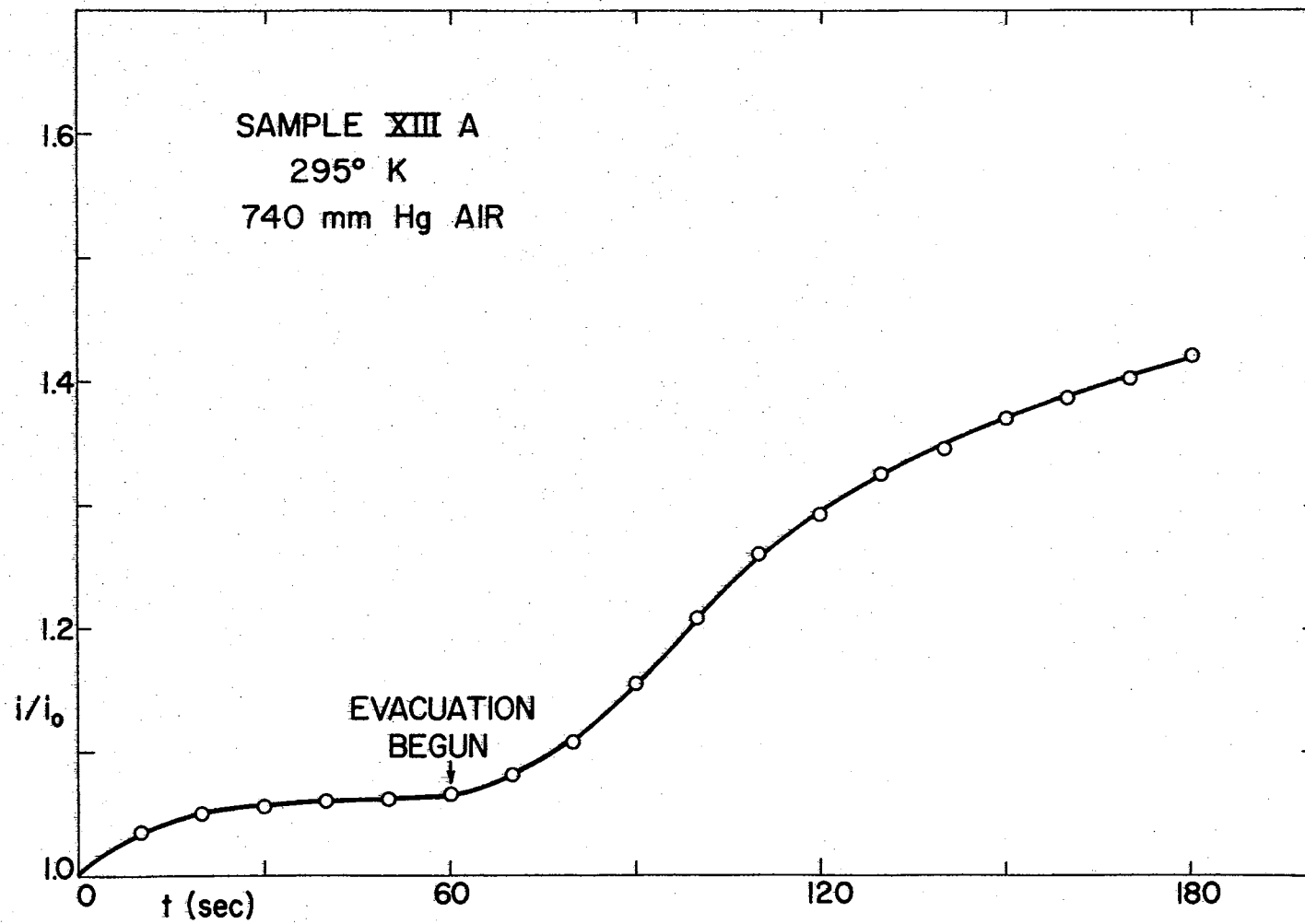


Figure 8. Effect of Removal of Air on Photocurrent Rise

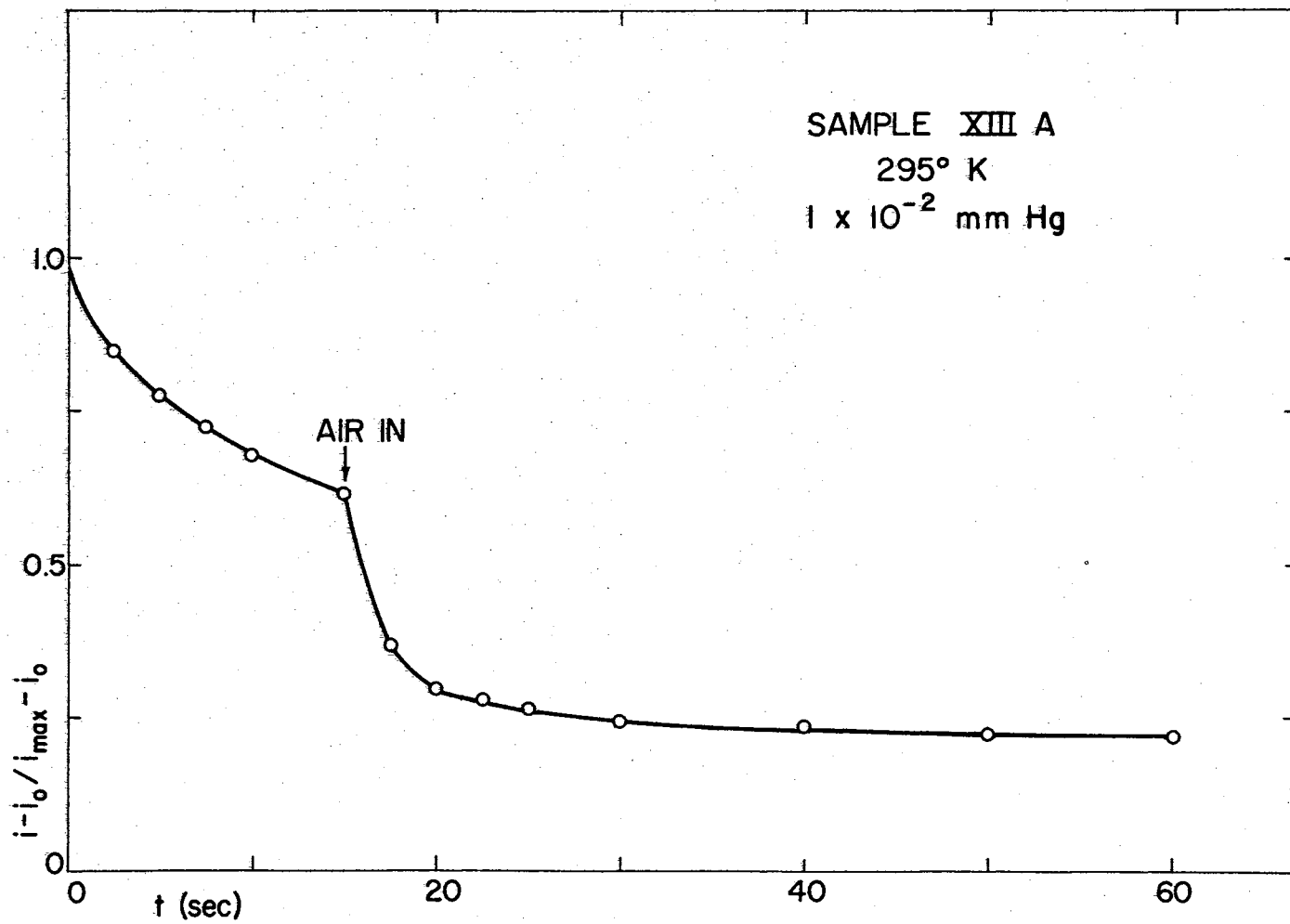


Figure 9. Effect of Admitting Air on Photocurrent Decay

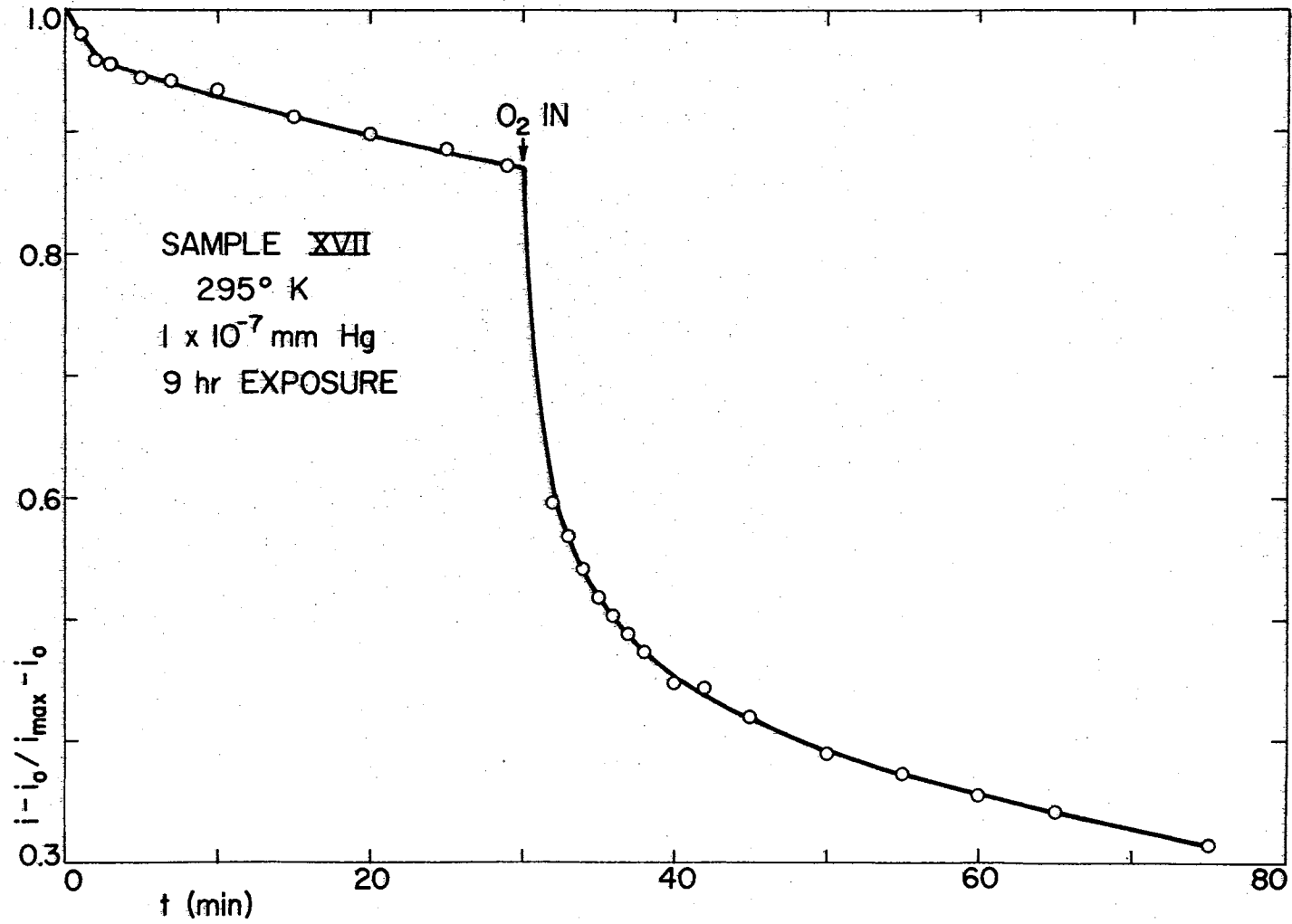


Figure 10. Effect of Oxygen Admission on Decay

fraction decayed, has been plotted. This decay is that which followed a nine-hour exposure of sample XVII to strong illumination in a vacuum maintained at  $1 \times 10^{-7}$  mm Hg. This vacuum was held during the first thirty minutes of the decay, at the end of which time the system was swept with oxygen gas for one minute and then filled to atmospheric pressure with the tank oxygen. The accelerated decay was linear with the logarithm of  $t$  for a period of roughly 75 minutes. The numerical results obtained in this experiment are given in Table II.

TABLE II  
EFFECT OF OXYGEN ON DECAY PARAMETERS OF SAMPLE XVII

Exposure length in vacuum	= 540 minutes
$n_t/n_0$	= 1.328
Decay slope* in vacuum	= 0.032
Fraction decayed after 30 min in vacuum	= 0.131
Decay slope* in oxygen	= 0.466
Fraction decayed after first 30 min in $O_2$	= 0.645

$$*\text{Decay slope} = \frac{\Delta \left[ \frac{n_t - n}{n_t - n_0} \right]}{\Delta (\ln t)}$$

All curves in Figures 5 through 10 were obtained at room temperature. Figure 11 is a logarithmic plot of a decay at 99°K which was begun in a vacuum of  $1 \times 10^{-2}$  mm Hg and during which air was admitted to the system. The same acceleration of decay coincident with the entry of oxygen into the system is evident at this reduced temperature, although there is a definite reduction in the magnitude of the change of the decay rate below that seen at higher temperatures.



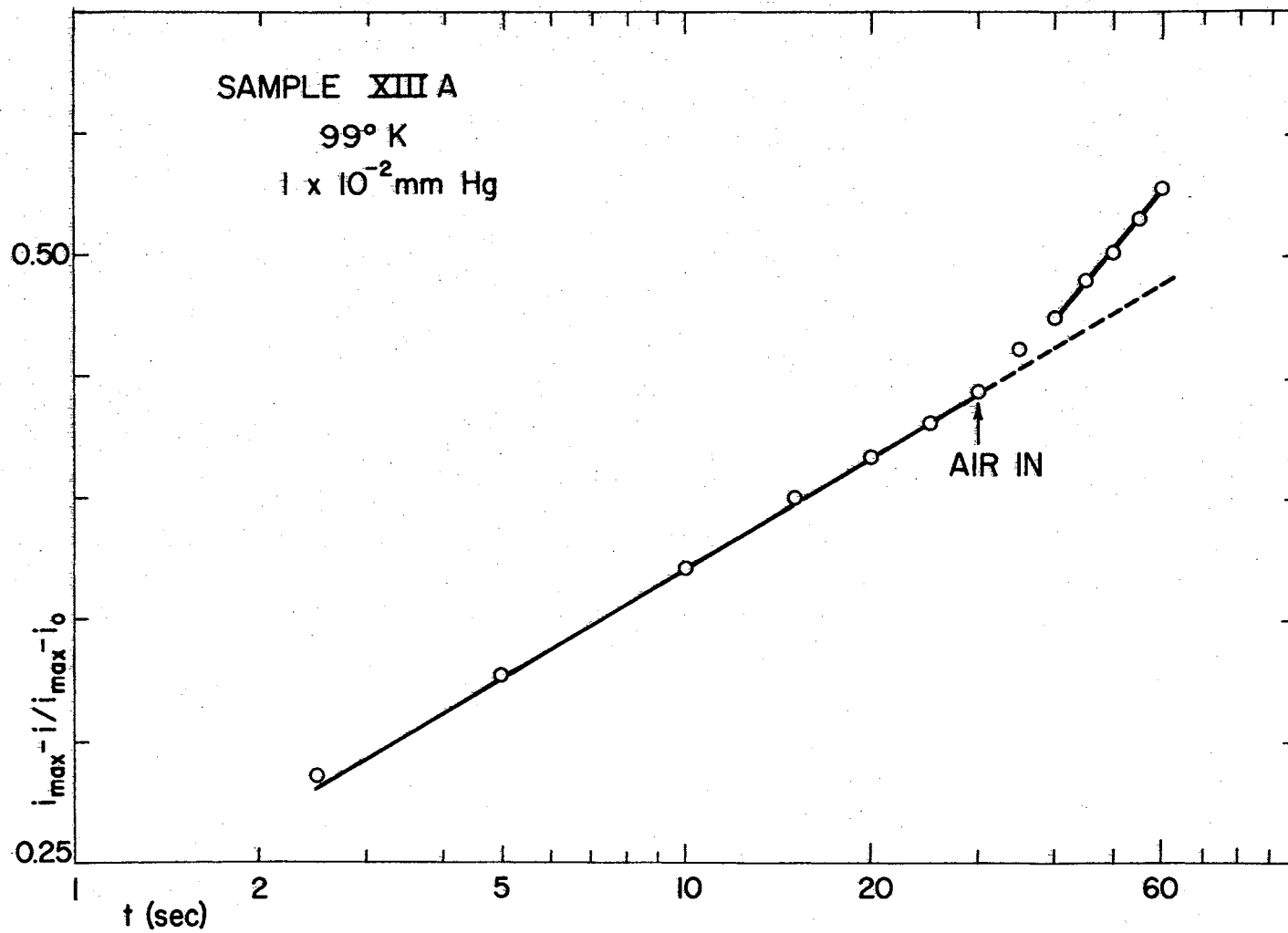


Figure 11. Effect of Admission of Air on Logarithmic Decay at Low Temperature

The effects of admitting air during a decay begun in vacuum, using the same sample, are compared in Table III (see page 51). It can be seen that the same general behavior prevails over the temperature range investigated. Further detailing of temperature effects as such will be deferred to the next section.

The results obtained using sample XIII A which have been presented up to this point followed a roughening of the broad faces of this sample. Originally polished as were all other natural samples, XIII A was ground to frosty appearance using 180 mesh alumina after it was found that it showed the usual response to ambient oxygen. A matched set of data from two short exposures and the following decays, taken under identical conditions except for the ambient, was obtained before roughening XIII A. Results are shown below in Table IV.

TABLE IV  
COMPARISON OF PHOTOCONDUCTIVE RESPONSE IN AIR AND  
VACUUM IN SAMPLE XIII A\* AT 325°K

Ambient	Dark current ( $\mu\text{a}$ )	Length of exposure (min)	$\frac{n_f}{n_0}$	$\frac{n_f - n}{n_f - n_0}$ (at 30 sec)	Decay slope**
740 mm Hg air	58.0	1.00	1.0035	0.473	0.147
$3 \times 10^{-3}$ mm Hg	58.0	1.00	1.0061	0.308	0.093

\*Polished surfaces

$$**\text{Decay slope} = \frac{\Delta \left( \frac{n_f - n}{n_f - n_0} \right)}{\Delta(\ln t)}$$

If the above decay slopes are compared with those in the third line of Table III, it can be seen that the roughening of the surface increased the sensitivity to oxygen somewhat. The change in surface area brought

TABLE III

EFFECT OF ADMITTING AIR AT SEVERAL TEMPERATURES (SAMPLE XIII A)

Pressure (mm Hg)	Temperature (°K)	Exposure time (min)	$\frac{n_f}{n_0}$	$t_1 - t_0^*$ (sec)	$\frac{n_f - n}{n_f - n_0}$ (at $t_1$ )	Decay slope** in vacuum	$t_2 - t_1^*$ (sec)	$\frac{n_f - n}{n_f - n_0}$ (at $t_2$ )	Decay slope** in air
$1 \times 10^{-2}$	99	1.00	$\approx 200$	30	0.444	0.064	30	0.528	0.121
$3 \times 10^{-3}$	298	1.00	1.344	191	0.773	0.090	40	0.857	0.576
$3 \times 10^{-3}$	323	0.75	1.121	31	0.519	0.136	15	0.740	0.302

\* $t_0$  = time at which decay began $t_1$  = time at which air admitted $t_2$  = time at which last data point taken

$$**\text{Decay slope} = \frac{\Delta \left( \frac{n_f - n}{n_f - n_0} \right)}{\Delta (\ln t)}$$

about by the roughening was probably an increase by a factor of not more than three. Such an increase in surface area would be sufficient to account for the observed changes in response to oxygen.

The results of a series of measurements on sample III, all involving thirty-second exposures at the same intensity of illumination, are given in Table V.

TABLE V  
EFFECT OF AMBIENT ON RESPONSE OF SAMPLE III

Ambient	Temperature (°K)	$\frac{n_p}{n_0}$	$\frac{n_p - n}{n_p - n_0}$ (at 30 sec)	Decay slope*
$7.5 \times 10^{-6}$ mm Hg	297	1.521	0.324	0.067
$8 \times 10^{-6}$ mm Hg	296	1.626	0.314	0.062
740 mm Hg air	296	1.341	0.750	0.119
740 mm Hg air	297	1.343	0.688	0.111
740 mm Hg air	326	1.091	0.630	0.067
740 mm Hg air	346	1.045	0.844	0.137
740 mm Hg air	270	1.617	0.797	0.122

$$*\text{Decay slope} = \frac{\Delta \left( \frac{n_p - n}{n_p - n_0} \right)}{\Delta (\ln t)}$$

These figures indicate that sample III is affected by oxygen in the same manner as samples IV, XIII A, and XVII. In addition, the top four lines show the degree of reproducibility experienced in measurements of the type employed. Errors in data reduction were usually less than  $\pm 2$  per cent, although in some cases circuit noise or a rapid change of current made allowances of up to  $\pm 4$  per cent necessary. Other deviations

stemmed from the contacts, the state of the sample, and possibly contaminants in the ambient.

Difficulties originating in the contacts were distinguishable by large changes of the dark resistance and/or the onset of noise. The chance of getting anomalous results because of the state of the sample was virtually eliminated by allowing sufficient time for decay to go to completion, and for the dark current to remain in equilibrium in the dark for a period of several hours before beginning another experiment. The possibility of a contaminated ambient was greatest when the ambient used was air. Checks made with sample IV in dry oxygen and unfiltered air indicated not only that there was ordinarily little in the air to alter the quantities being measured but that the effect of oxygen on the sample was essentially saturated at an oxygen pressure of 150 mm Hg or less. Rise curves in these two ambients duplicated one another with deviations not exceeding two per cent during five-minute exposures. Other tests with mercury vapor and water vapor indicated that the usual experimental concentrations of these gases are of little or no consequence in determining the surface behavior of stannic oxide at room temperature.

In experiments covering an hour or more, temperature fluctuations often caused some undesirable--though minor--effects such as drifts in the saturation photocurrent. Experiments of excessive length were the exception rather than the rule, however, and were totally impractical at temperatures other than room temperature,

The results of a series of five-minute exposures of sample XVII at room temperature are listed in Table VI. Data in this series were taken by the four-contact method. These results reveal no clear-cut

TABLE VI  
EFFECT OF AMBIENT ON PHOTORESPONSE OF SAMPLE XVII

Ambient	$\frac{n_s}{n_0}$	$\frac{n_s - n}{n_s - n_0}$ (at 25 min)
740 mm Hg air	1.035	0.503
740 mm Hg dry air	1.025	0.580
740 mm Hg dry O <sub>2</sub>	1.0275	0.531
6 x 10 <sup>-6</sup> mm Hg	1.026	0.350
1 x 10 <sup>-7</sup> mm Hg	1.0225	0.248

trends other than the hastening of decay by the presence of an oxygen-rich ambient. Note that for this particular specimen, the effect of the presence of oxygen was negligible for the determination of rise parameters.

A similar scatter appears in Table VII, which lists the rise and decay parameters measured for sample IV in extended exposures in helium at atmospheric pressure followed by a decay in helium and an additional decay when oxygen was introduced. As in the above table, all data were obtained at room temperature using the four-contact method.

TABLE VII  
EFFECT OF AMBIENT ON PHOTORESPONSE OF SAMPLE IV

Exposure time (min)	$\frac{n_s}{n_0}$	t <sub>1</sub> <sup>*</sup> (min)	Second ambient	Decay slope <sup>**</sup> (He)	Decay slope <sup>**</sup> (O <sub>2</sub> )
420	1.062	41	Dry O <sub>2</sub>	0.065	0.348
420	1.115	25	Dry O <sub>2</sub>	0.009	0.303
486	1.091	45	Wet O <sub>2</sub>	0.050	0.380
570	1.095	15	Dry O <sub>2</sub>	0.018	0.213

\*Time at which O<sub>2</sub> entered system

$$**\text{Decay slope} = \frac{\Delta \left( \frac{n_s - n}{n_s - n_0} \right)}{\Delta (\ln t)}$$

The general characteristics of the photoconductive responses in the artificial samples differ rather markedly from those observed with the natural samples. At room temperature, the photocurrent rise in the artificial samples is quite rapid, the photocurrent reaching saturation within fifteen seconds or less. The decay is even more rapid, going to completion in 0.1 sec or less. The low conductivity of these samples, in the range between  $10^{-7}$  ohm<sup>-1</sup>-cm<sup>-1</sup> and  $10^{-8}$  ohm<sup>-1</sup>-cm<sup>-1</sup>, and their needle-like shape tend to give individual specimens resistances up to  $10^{10}$  ohms. Consequently, measured dark currents were very low, often 0.01  $\mu$ a or less. However, photocurrents of several microamperes resulted from ultraviolet illumination of the same type and intensity as that used in work on the natural samples, giving values of  $n_t/n_0$  two to three orders of magnitude greater than those measured for natural samples. A typical rise and decay curve for an artificial sample is shown in Figure 12. Results of this type were obtained for samples GI, GII, GIII, GIV, GXIII, GXX, and GXXII, all at room temperature.

In attempts to detect a dependence of the photoresponse of these samples on the ambient, the responses of samples GI and GXXII were compared in air, oxygen, and vacuum. No effect was seen in GI at oxygen pressures ranging from 740 mm Hg to  $5 \times 10^{-8}$  mm Hg or in GXXII between the same upper limit and  $6 \times 10^{-8}$  mm Hg. These measurements were also at room temperature.

The surfaces of two artificial samples, GII and GXXII, were roughened to a microscopically frosty appearance using a 600 mesh alumina abrasive. After a thorough cleaning, further measurements of their conductivity and photoconductivity were made. In both samples the end-to-end resistance was reduced to less than  $10^7$  ohms, indicating

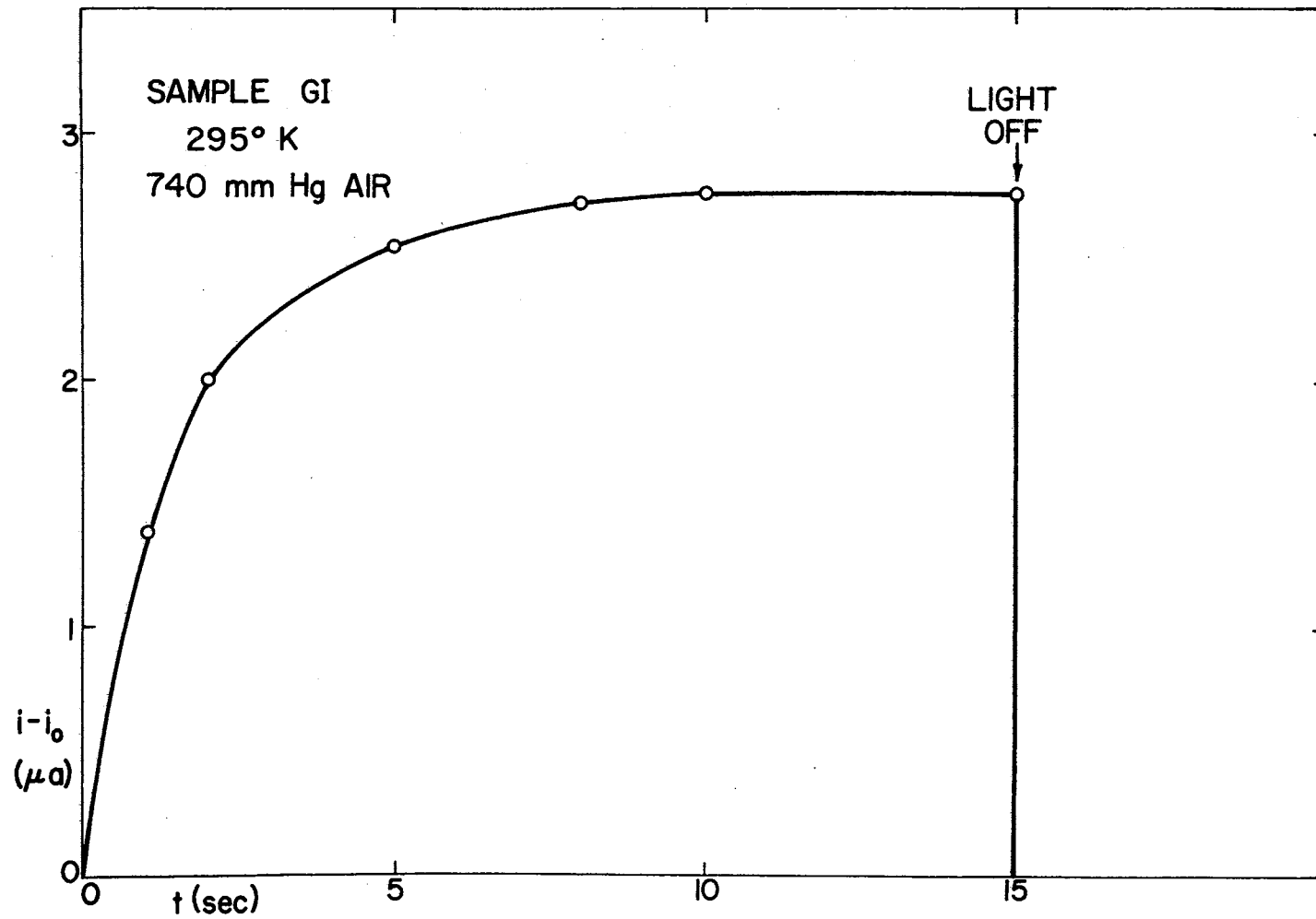


Figure 12. Typical Rise and Decay of Photocurrent for an Artificial Sample



that the surface layer removed had played a very appreciable role in determining the resistance of the specimens. A bulk conductivity of  $10^{-4}$  to  $10^{-3}$   $\text{ohm}^{-1}\text{-cm}^{-1}$  made these samples comparable with the natural samples in that respect. They were also found to more closely resemble the natural samples in photoresponse, including slow rise and decay and values of  $n_f/n_0$  not greatly exceeding unity. The results of tests in various ambients are given in Table VIII.

TABLE VIII  
EFFECT OF AMBIENT ON PHOTORESPONSE OF ARTIFICIAL  
SAMPLES HAVING ROUGHENED SURFACES

Sample	Ambient*	$\frac{n_f}{n_0}$	$\frac{n_f - n}{n_f + n_0}$ (at 30 sec)
GII	Air	1.044	0.512
GII	O <sub>2</sub>	1.034	0.524
GII	$7.5 \times 10^{-8}$ mm Hg	1.071	0.352
GXXII	Air	1.102	0.426
GXXII	$1 \times 10^{-6}$ mm Hg	1.144	0.385

\*At atmospheric pressure unless specified otherwise.

All exposures in the above two series were of one minute's duration, and no change in illumination was made either in the series of experiments involving sample GII or in that involving sample GXXII.

The photocurrent decay in artificial samples on which the surfaces had not been roughened was found to be slowed by lowering the temperature of the sample. At temperatures below 200°K the decay was sufficiently slow to allow measurement of the effect of changing the ambient during decay. Several trials with sample GI showed no evidence of an increase

in the decay rate coincident with the entry of oxygen into the system as was observed with natural samples.

#### Effect of Temperature on Photoconductivity

The response of samples III, IV, and XIII A has been measured as a function of temperature as well as of ambient. In a number of cases the effects of temperature and ambient were measured simultaneously. For this reason, there will be occasional reference in this section to tables and figures appearing in the preceding section.

The photocurrents generated in sample IV by one-minute exposures at several temperature points are plotted in Figure 13, along with two points taken from one-minute exposures of sample XIII A. All data for sample IV were obtained under the same illumination, and both points for sample XIII A were for like illumination. Photocurrents were plotted instead of the usual ratio because of the variation of dark conductivity with temperature. An example of the very high values of  $n_f/n_0$  measured at low temperatures can be seen in the first line of Table III. Values exceeding 100 were typical for samples IV and XIII A in the temperature range near  $100^\circ\text{K}$ . Unlike samples IV and XIII A, sample III showed a flat photocurrent vs temperature curve between  $296$  and  $346^\circ\text{K}$ , with a distinct drop between  $296$  and  $270^\circ\text{K}$ , the photocurrent at  $270^\circ\text{K}$  being less than half the corresponding photocurrent at  $296^\circ\text{K}$ .

The effect of temperature on the logarithmic decay rate is illustrated in Figure 14, in which several decays over a broad range of temperature are plotted. All curves in Figure 14 followed one-minute exposures in air at atmospheric pressure. A similar set of curves for

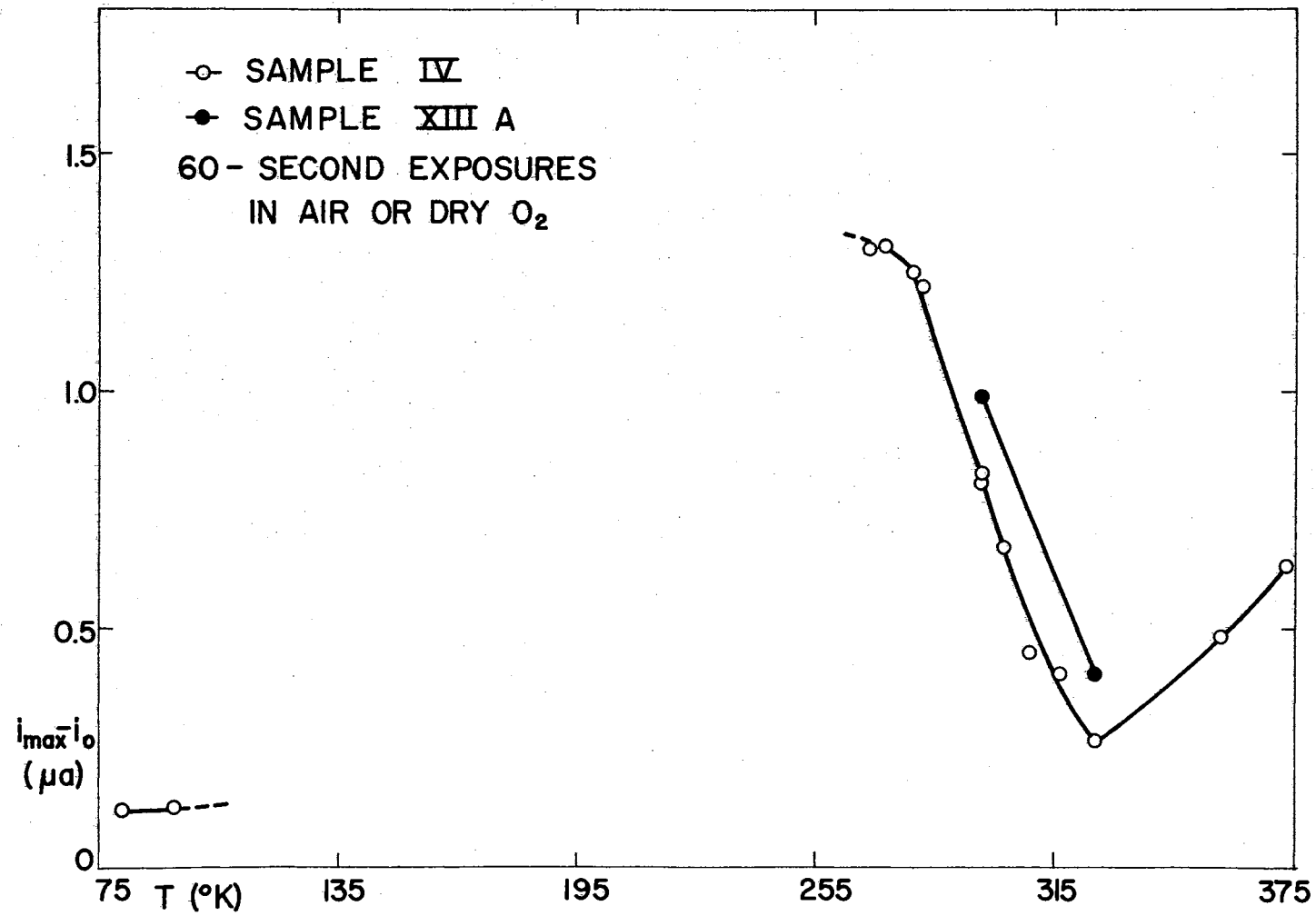


Figure 13. Photoresponse vs Temperature

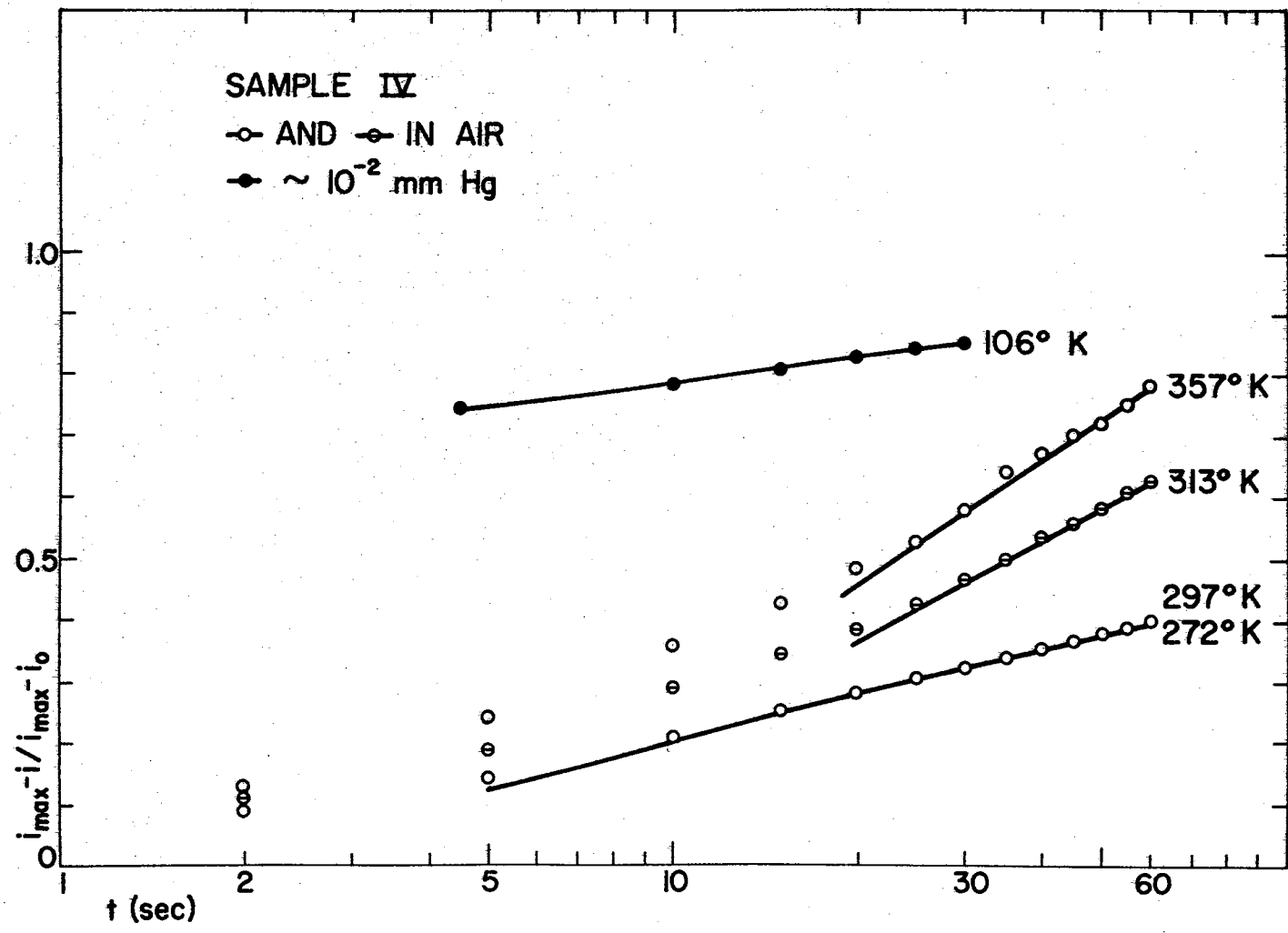


Figure 14. Logarithmic Decays for Sample IV at Several Temperatures

sample XIII A, also following one-minute exposures but with a vacuum of  $3 \times 10^{-3}$  mm. Hg as the ambient, is shown in Figure 15. This latter set of data was obtained before the surfaces of sample XIII A were roughened. In both samples the generally logarithmic character of the decay is not altered over the temperature ranges indicated, the slope of the decay curve shows little change between roughly  $100^{\circ}\text{K}$  and room temperature, and there is a tendency of this slope to increase at higher temperatures, particularly in sample IV. Some temperature effect data for sample III are included in Table V and although contradictory decay results appeared at  $326^{\circ}\text{K}$  and  $346^{\circ}\text{K}$  for this sample, general trends indicate that the decay slope at  $346^{\circ}\text{K}$  is the more likely of the two to be correct. On this basis the same slight acceleration of decay above  $310^{\circ}\text{K}$  is also present in sample III.

It was also noted that at low temperatures the initial rate of photocurrent decay was dependent upon the duration of the exposure. Two relatively short exposures, one of five times the duration of the other, are shown in Figure 16. Both are for sample IV in vacuum, the one-minute exposure being at  $110^{\circ}\text{K}$  and the five-minute exposure at  $88^{\circ}\text{K}$  under a higher illumination intensity. Additional evidence of this effect is given in Table IX.

Table IX shows not only that decay rates are slowed by lengthening the period of illumination, but that the roughening of the broad faces of sample XIII A also acted so as to retard decay at low temperatures.

The logarithmic decay illustrated in Figure 14 is not linear during the first seconds of the decay. This deviation from linearity is commonplace except at low temperatures. If a constant is added to the time coordinate at each data point--in effect shifting the entire curve

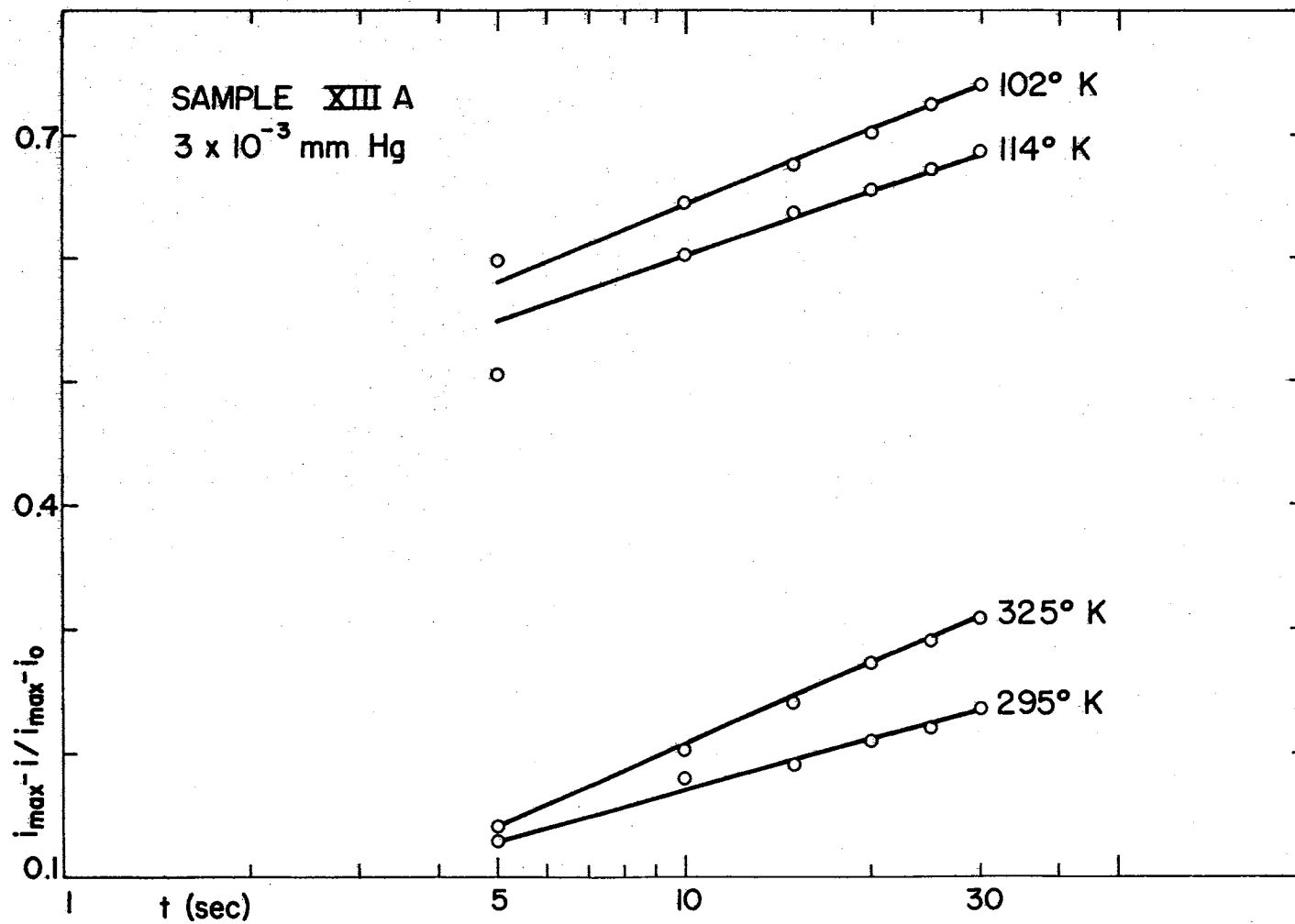


Figure 15. Logarithmic Decays for Sample XIII A at Several Temperatures

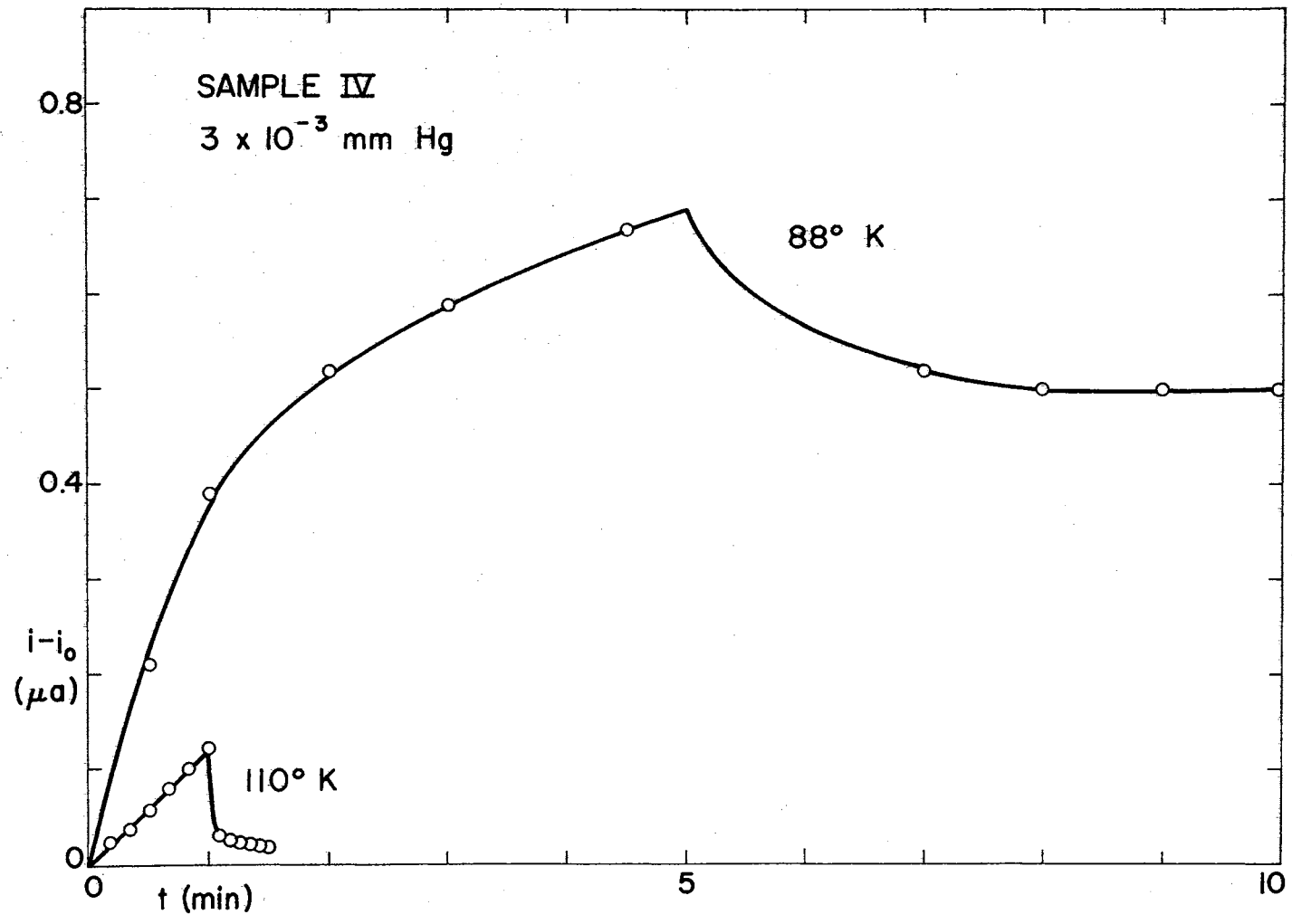


Figure 16. Typical Rise and Decay Curves for a Natural Sample at Low Temperatures

TABLE IX  
COMPARISON OF PHOTOCURRENT DECAYS AT LOW TEMPERATURE

Sample	Ambient*	Temperature (°K)	Exposure time (min)	$\frac{n_f - n}{n_f - n_0}$ (at 30 sec)
XIIIA (rough)	$3 \times 10^{-3}$ mm Hg	94	1.00	0.286
XIIIA (rough)	$1 \times 10^{-2}$ mm Hg	99	0.50	0.444
XIIIA (rough)	$3 \times 10^{-3}$ mm Hg	102	1.00	0.742
XIIIA (rough)	$3 \times 10^{-3}$ mm Hg	109	0.75	0.800
XIIIA (smooth)	$3 \times 10^{-3}$ mm Hg	114	1.00	0.686
IV	$3 \times 10^{-3}$ mm Hg	106	1.00	0.852
IV	$1 \times 10^{-4}$ mm Hg	88	5.00	0.119
IV	Dry O <sub>2</sub>	81	5.00	0.196
IV	Dry O <sub>2</sub>	95	5.00	0.140
IV	Dry N <sub>2</sub>	85	5.00	0.151
IV	He	136	5.00	0.059
IV	He	139	5.00	0.083
IV	He	146	10.00	0.018
IV	He	146	10.00	0.044

\*Ambient at atmospheric pressure unless specified otherwise.



to the right--the curve becomes linear throughout. The additive factor required must be determined individually for each curve, and is the measure of the quantity  $t_d$  of Equation 17. The measured values of  $t_d$  and the decay slopes of the linearized logarithmic decay curves for sample IV following identical one-minute exposures in air at atmospheric pressure are given in Table X. These numbers show that both quantities increase over the temperature range between 270°K and 350°K. On the basis of general consistency, the data for decays at 269°K and 313°K seem highly questionable and may well have been the result of temperature instability. Furthermore, the trends observed in other samples were of the same nature.

Another effect noted in the logarithmic decay curves was the drop below linearity beginning before completion of the decay. In some cases this occurred with the decay considerably less than fifty per cent complete. The best example of this that has appeared in the curves thus far shown in the various figures is the decay in oxygen of sample IV shown in Figure 7. It was noted that there was a relationship between the time required for this effect to become noticeable and the illumination period. This is best represented, however, as a systematic dependence on the ratio  $\Delta n/n_i$ , where  $\Delta n = n_i - n(t)$  is now understood to represent the decrease in carrier density up to the time of onset of sublinearity. The dependence is illustrated in Table XI. Except in sample IV, the room temperature value of  $\Delta n/n_i$  lies between 0.1 and 0.2. Also note that for equal exposure times in both sample III and sample IV there is a definite decrease in  $\Delta n/n_i$  as temperature increases.

The response of artificial sample GI was measured over the temperature range between 122°K and room temperature. While the character of

TABLE X  
 DECAY PARAMETERS FOR SAMPLE IV IN AIR

Temperature (°K)	$t_d$ (sec)	Decay slope*
269	3.9	0.142
272	2.0	0.112
280	2.0	0.097
281	2.0	0.110
297	2.3	0.120
302	2.2	0.125
303	2.2	0.132
304	2.3	0.141
309	2.3	0.147
313	10.0	0.295
325	4.0	0.165
357	6.0	0.311

$$*\text{Decay slope} = \frac{\Delta \left( \frac{n_t - n}{n_t - n_0} \right)}{\Delta (\ln t)}$$

TABLE XI  
 PARAMETERS ASSOCIATED WITH THE ONSET OF SUBLINEARITY  
 IN LOGARITHMIC DECAY CURVES

Sample	Ambient	Temperature (°K)	Exposure time	$\frac{\Delta n}{n_p}$	t*
III	Air	270	30 sec	0.29	20-25 sec
III	Air	296	30 sec	0.18	20-25 sec
III	Air	309	30 sec	0.12	20-25 sec
IV	Air	272	1 min	0.127	45-60 sec
IV	Air	280	1 min	0.061	45-60 sec
IV	Air	281	1 min	0.066	45-60 sec
IV	Air (4 curves)	297-298	1 min	0.022 ±0.002	45-60 sec
IV	Air	297	50 min	0.034	90 min
IV	Air	297	500 min**	0.037	85 min
IV	Air	309	1 min	0.015	45-60 sec
IV	Air	317	1 min	0.01	45-60 sec
VIII B	O <sub>2</sub>	297	10 min	0.14	22 sec
VIII B	Vacuum	297	10 min	0.11	20 sec
XVII	O <sub>2</sub>	297	540 min**	0.176	75 min

\*t = time of onset of sublinearity, measured from start of decay

\*\*photocurrent reached saturation

the rise was not seen to change appreciably, the decay curves showed a considerable decrease in decay rate at low temperatures. This decrease was perceptible at 239°K, the decay taking about five seconds to go to completion at that temperature. At 250°K the decay was complete within less than one second, essentially the sharp drop shown in Figure 12.

Figure 17 shows the logarithmic decay curves for sample GI at several reduced temperatures. Note that none are linear, but note also that  $(n_f - n)/(n_f - n_0)$ , which is equal to  $\Delta n/n_f$  to within one per cent, is large for all data points. The possibility remains that earlier portions of these curves were linear, but sufficiently accurate data reduction to prove or disprove this supposition was impractical on the steep early parts of the decays.

Rise curves at low temperatures saturated quickly as did room temperature rise curves. Under the same illumination, the saturation photocurrent measured for sample GI was 0.75  $\mu\text{a}$  at 122°K and 0.83  $\mu\text{a}$  at 298°K, the applied voltage being 40 V in both cases.

Sample GI, which retained its original surfaces, showed no sensitivity to the ambient at any temperature. The effect of lowered temperature on the ambient dependence in the natural samples was to reduce it, though not completely eliminating it even near the liquid nitrogen point. This can be seen by comparing Figures 9, 10, and 11.

#### Oxidation and Reduction

Samples VI, VIIIA, and VIIIB were used in the oxidation and reduction experiments. These samples were chosen for their similar pre-treatment optical and electrical properties, and were originally parts of the same single crystal. Sample VIII, a comparatively large piece, was

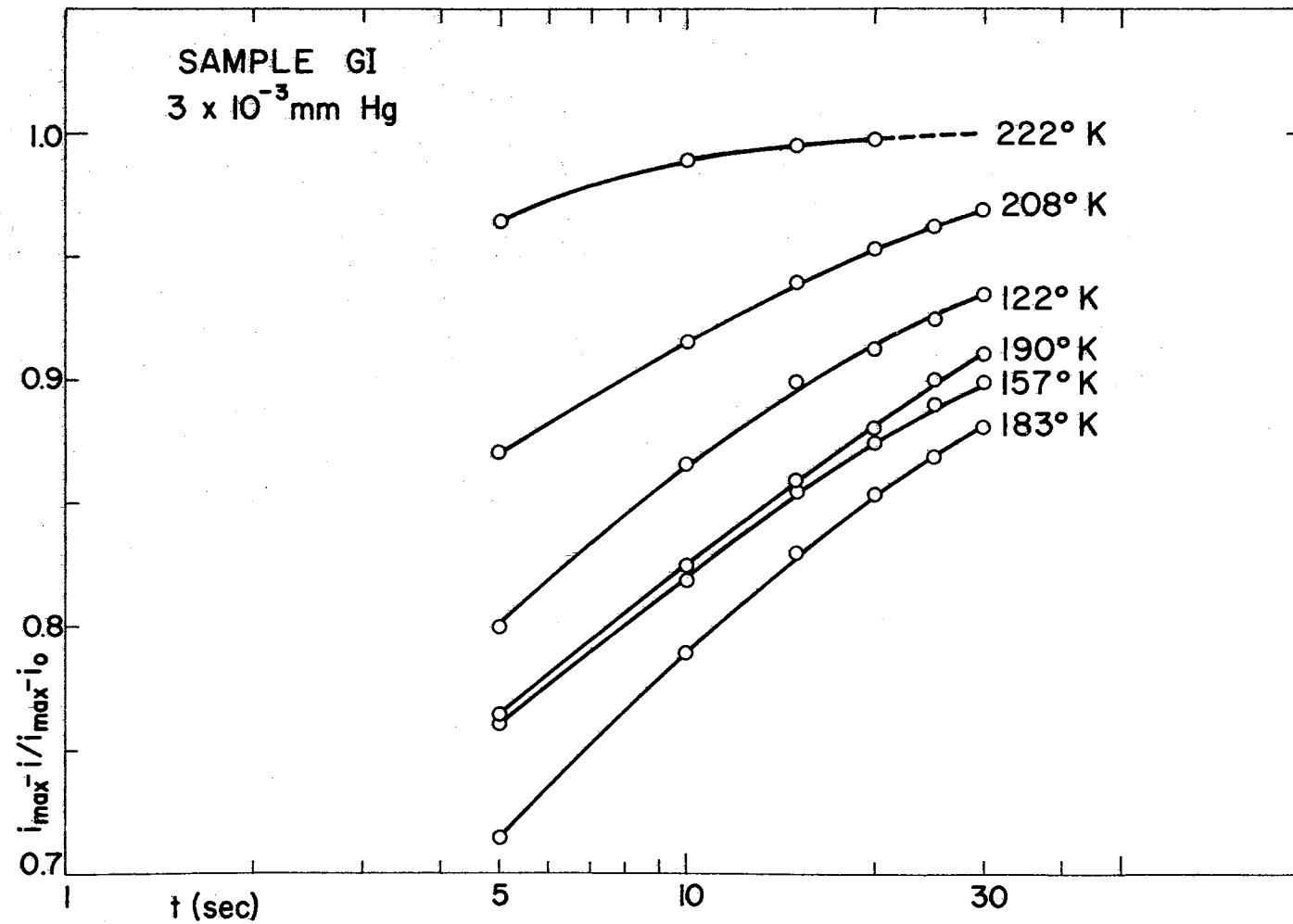


Figure 17. Effect of Temperature on Photocurrent Decay in a Typical Artificial Sample

divided into two pieces of approximately equal size for separate reduction experiments with hydrogen and vacuum.

Sample VI was heated in oxygen, VIIIA in hydrogen, and VIIIB in a vacuum of  $1 \times 10^{-3}$  mm Hg. The ambient in each case was kept in the system throughout the period of temperature increase, the 15-minute period of steady temperature near  $925^{\circ}\text{K}$ , and the following cooling period. The broad faces of sample VIIIB were later ground and polished to remove surface material so as to determine whether the observed changes were limited to the surface or penetrated to some depth within the sample. The thickness of material removed from each face was 0.032 mm. The effects of these treatments on the short wavelength cutoff and the dark conductivity are summarized in Table XII.

TABLE XII  
RESULTS OF OXIDATION AND REDUCTION EXPERIMENTS

Sample	Short wavelength cutoff ( $\mu$ )	Dark conductivity ( $\text{ohm}^{-1} \cdot \text{cm}^{-1}$ )
VI	350	$6.4 \times 10^{-6}$
VI( $\text{O}_2$ )	387	$7.2 \times 10^{-6}$
VIII	350	$1.1 \times 10^{-4}$
VIIIA( $\text{H}_2$ )	not available	$1.0 \times 10^{-7}$
VIIIB ( $1 \times 10^{-3}$ mm Hg)	380	$1.3 \times 10^{-6}$
VIIIB (after removal of surface material)	375	$3.2 \times 10^{-7}$

Other changes in all three samples were evident on inspection. The oxidized sample, VI, was nonuniformly colored throughout with a

yellow-orange deepening to rust red in scattered areas. The coloration did not greatly interfere with transparency, and there was no evidence of change in the surface polish. Samples VIIIA and VIIIB, reduced in hydrogen and rough vacuum respectively, both acquired a weak yellow-green tinge which appeared uniform in clear areas of these samples. Sample VIIIA also showed surface erosion, and for this reason accurate measurements of the short wavelength cutoff after reduction in hydrogen were not possible. Visual checks showed that this sample was still transparent to blue light, although no transmission at wavelengths shorter than 530 m $\mu$  was registered by spectrophotometer measurements due to light scattering.

In sample VIIIB, the removal of surface material did not produce any noticeable change in the yellow-green coloration. Based upon strictly geometric factors, the material removed had an average conductivity near  $10^{-10}$  ohm $^{-1}$ -cm $^{-1}$ .

Sample VIIIA was destroyed in a second hydrogen reduction experiment in which the heating time was increased to 150 minutes. By the end of this period the specimen had completely decomposed.

In sample VIIIB there was a noticeable change in the photoresponse following reduction in vacuum. The removal of surface material later brought about a near restoration of the pre-reduction characteristics. The major change following the reduction was a sharp increase in both the rates of rise and decay during the initial seconds of rise and decay. Logarithmic plots of decay curves before reduction, shortly after reduction, and following the removal of surface material are shown in Figure 18.

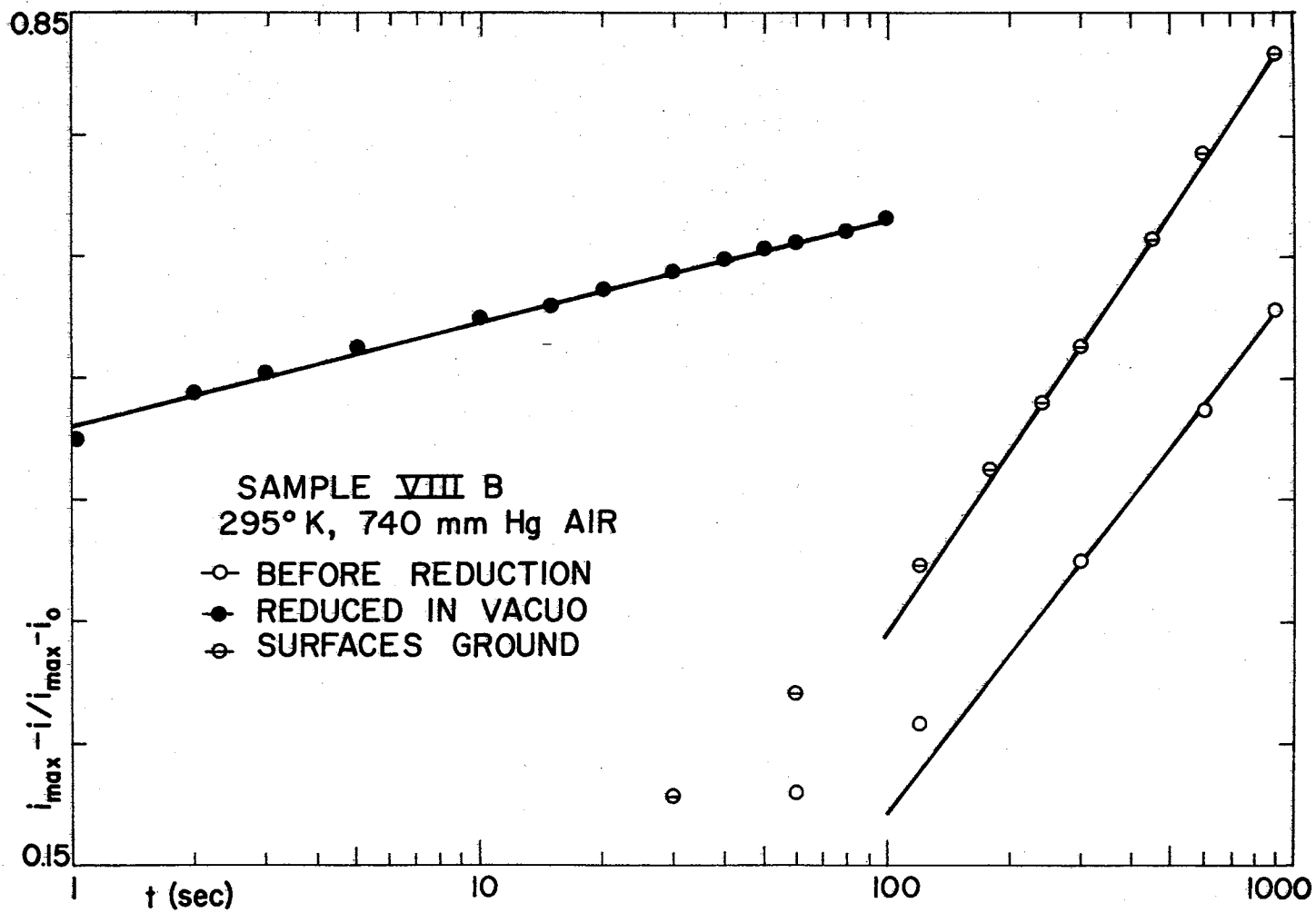


Figure 18. Effects of Reduction and Surface Abrasion on Decay in Sample VIII B



A similar acceleration of the initial parts of the rise and decay curves was noted in sample VIIIA following reduction in hydrogen. This specimen also showed a considerable increase in contact noise.

Sample VI did not show any increase in the initial rate of rise or decay, but retained the slow response typical of untreated natural samples.

None of these samples exhibited the usual sensitivity to the ambient following oxidation or reduction. A slight dependence of the response of sample VIIIB on the ambient was detected beyond question by observing the effect of changing the ambient during the decay, in the manner of the experiment represented in Figure 9. In the case of VIIIB the rate change observed was not more than about ten per cent. The removal of surface material had no noticeable effect. Table XIII illustrates the reduced ambient dependence in sample VIIIB following vacuum reduction. All experiments were at room temperature.

TABLE XIII

TYPICAL RISE AND DECAY PARAMETERS OF SAMPLE VIIIB  
FOLLOWING REDUCTION IN VACUUM

Ambient*	Dark** current ( $\mu$ a)	Length of exposure (min)	$\frac{n_f}{n_0}$	Decay slope***	$\frac{n_f - n}{n_f - n_0}$ (at 90 min)
He	0.72	30	5.139	0.136	0.685
He	0.71	60	5.352	0.141	0.709
Air	0.73	30	4.507	0.135	0.691

\*All ambients at atmospheric pressure

\*\*With 67.5 V applied

$$***\text{Decay slope} = \frac{\Delta \left( \frac{n_f - n}{n_f - n_0} \right)}{\Delta (\ln t)}$$

Effect of the Ambient on Dark Conductivity and  
Contact Potential

The dark conductivity of samples IV and XVII were measured potentiometrically in air, oxygen, helium, and vacua of  $1 \times 10^{-3}$  mm Hg or less. All measurements were made at room temperature and with the sample having been shielded from illumination for a period of sufficient length to allow any photoconductivity to decay completely. Frequent measurements were centered around the times at which ambients were changed but revealed no dark conductivity changes in either sample. Any long term changes were so small as to be masked by minor variations caused by fluctuations in the temperature of the sample.

Samples VI, VII, and X were used in contact potential measurements. Sample VI had been oxidized before these measurements were made. As in the dark conductivity experiments, there were no perceptible changes noted upon change of ambient. A slow drift of the measured potential often occurred. An example of the drift, along with the insensitivity to oxygen pressure, appears in Table XIV.

TABLE XIV

CONTACT POTENTIAL MEASUREMENTS FOR SAMPLE VII

t (min)	$\Delta V(V)$	Ambient
0	3.78	740 mm Hg air
18	3.78	740 mm Hg air
47	3.78	740 mm Hg air
131	3.81	740 mm Hg air
135	--	evacuation begun
136	3.83	0.01 mm Hg
141	3.84	$10^{-3}$ mm Hg
150	3.84	$10^{-3}$ mm Hg
168	3.86	$10^{-3}$ mm Hg
303	3.87	$10^{-3}$ mm Hg

Both upward and downward drifts were found to show no measurable response to the entry of oxygen into the system or its removal from the system, nor was any effect noted when  $\Delta V$  was not varying. This was true for all three samples. Values of  $\Delta V$  indicated the sample to be positive with respect to the platinum reference electrode, with sample VII showing a greater  $\Delta V$  than the other two samples both of which gave a  $\Delta V$  of slightly more than one volt. In view of the scatter in the measured values of  $\Delta V$ , these magnitudes are considered less significant than the fact that they showed no essential dependence upon ambient change. Possible sources of error include contaminants on either the sample or the reference electrode, the presence of electrostatic charge on the glass of the bell jar or on one or more of the insulating materials used in the construction of the sample holder, or pickup in the detection circuit.

#### Wavelength Dependence of Photoconductivity

The rapid rise and decay of photoconductivity in the artificial samples enabled a comparison of responses at the wavelengths of the strong mercury lines to be made by an unbroken scan through the wavelength region of interest. Such scans for samples GIII, GIV, GXIII, GXX, and GXXII resulted in the composite plot of relative quantum efficiencies in Figure 19. The absence of any data on carrier densities for these samples prevented the calculation of absolute quantum efficiencies.

The peak response for these five artificial samples is seen to be in the wavelength range between 310  $m\mu$  and 320  $m\mu$ , which corresponds to an energy difference of approximately 3.9 eV.

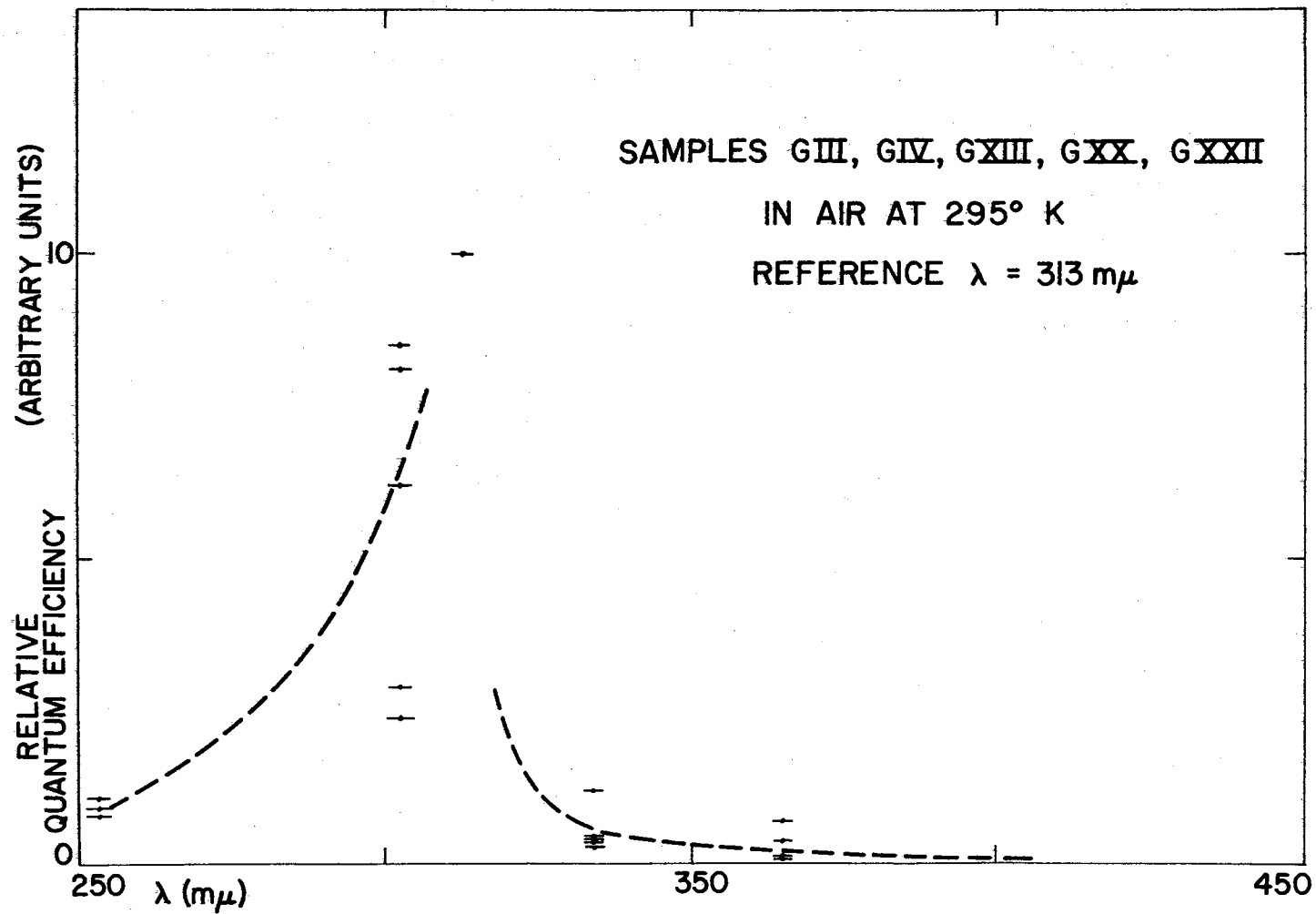


Figure 19. Photoresponse vs Wavelength for Artificial Samples

Comparable measurements were attempted with a number of the natural samples. Because of their slow responses only a general idea of their relative photoresponses at various wavelengths could be obtained. The natural samples checked were III, VI (after oxidation), VIIIIB (after reduction in vacuum), XIII A, XX, and XXIIB, which represented four different pieces of original material. All showed the same general distribution of sensitivity as was observed in the artificial samples.

Sample II was also checked under the same conditions as were the above samples but the peculiarities of this specimen warrant a more detailed description which will be taken up in the next section. All measurements were in air at room temperature, some with the contacts illuminated and some with the contacts shielded from any direct illumination. Response was the same in both cases.

#### Effects of Indium Diffusion

Sample II, in addition to having a dark conductivity lower than that of the other natural samples, showed unusually high sensitivity to illumination and a wavelength dependence of photoresponse unlike that seen in other natural samples or in artificial samples. The peak response observed in sample II was at 365-366  $m\mu$ , with the 313  $m\mu$  response being considerably weaker. Furthermore, this sample showed weak response to visible wavelengths up to 620  $m\mu$ . Other samples had shown weak response at 365-366  $m\mu$  but no detectable response at longer wavelengths.

In earlier work, this sample had been heated to near 1050°K with indium metal used as the contact material in measurements of

conductivity as a function of temperature. (24). On the supposition that some indium had diffused into the sample during the conductivity measurements, the surfaces were ground down by 0.037 mm each and the dark conductivity and wavelength response of photoconductivity again checked. The dark conductivity was found to have increased from  $6.3 \times 10^{-7} \text{ ohm}^{-1}\text{-cm}^{-1}$  to  $2.4 \times 10^{-6} \text{ ohm}^{-1}\text{-cm}^{-1}$  and the photoresponse peak had shifted to near 310 m $\mu$ , as seen in the other samples described in the last section. However, the unusually high photosensitivity (for a natural sample) and the weak response in the visible region remained, apparently little changed by the surface modification. Following these measurements, sample II was once again heated to near 1000°K in vacuum while clamped in contact with two small sheets of indium between two quartz plates. The peak photoresponse was shifted back to near 365 m $\mu$  and the dark conductivity lowered to  $8 \times 10^{-7} \text{ ohm}^{-1}\text{-cm}^{-1}$ , while the long wavelength response remained.

The indium treatment was repeated using another smaller natural sample from a different crystal, sample XXIIB. Before heating with indium, this sample showed the same wavelength dependence as was observed in the majority of the samples checked. Following the indium diffusion treatment, the conductivity was found to have been decreased by nearly three orders of magnitude and the photoresponse to have been almost entirely eliminated. From the very weak responses measured, there appeared to be no great difference between the sensitivity at 313 m $\mu$  and that at 365 m $\mu$ .

#### Other Work

The approximate ratio of bulk conductivity to surface conductivity

for natural samples was found to be of the order of 10. In concurrent measurements on other natural samples using a guard ring technique, J. Houston also found the bulk to be 10 to 100 times more conductive than the surface. If allowances are made for inhomogeneities in the natural samples, the bulk-surface conductivity ratio may be considerably greater than 10.

Attempts to detect evidence of thermally stimulated current to identify shallow trapping levels gave negative results both for natural samples IV and XIII A and for artificial sample GI.

In other low temperature work, short-period temperature cycling over a range of ten degrees or less during photocurrent decay showed that in the region of  $150^{\circ}\text{K}$  the mobility of carriers in sample GI, a typical artificial sample, increases with increasing temperature. The current changes noted were larger than any dark current between  $120^{\circ}\text{K}$  and  $300^{\circ}\text{K}$  by a factor of at least ten, ruling out the possibility of carrier density changes.

All artificial samples on which photoconductivity measurements were carried out were found to exhibit an approximately logarithmic decay of photocurrent during extended periods of illumination, with a stable level of photocurrent considerably below the original saturation photocurrent being attained after several hours continuous illumination. Blockage of the incident light at any time during this slow decay resulted in the usual quick decay. This was observed also in artificial samples having ground surfaces, though to a lesser extent. Similar effects were never noted in natural samples.

## CHAPTER V

### DISCUSSION AND CONCLUSIONS

#### Summary of Results

In the present investigation the following effects have been observed in samples of natural stannic oxide:

- (a) suppression of magnitudes and alteration of time rates of photoresponse by the presence of oxygen in the gaseous ambient at temperatures from  $99^{\circ}\text{K}$  to  $325^{\circ}\text{K}$ , the effects being more pronounced at higher temperatures
- (b) photocurrent decays logarithmic with time
- (c) more rapid photocurrent decays at low temperatures; otherwise no change in character of this aspect of the photoresponse between  $81^{\circ}\text{K}$  and  $373^{\circ}\text{K}$
- (d) decrease of initial decay rate with increasing exposure time at low temperature
- (e) no measurable dependence of contact potential or dark conductivity on ambient at room temperature
- (f) surface dark conductance lower than bulk dark conductivity by a factor of at least ten
- (g) lessening of over-all conductivity by one order of magnitude by oxidation and by three to four orders of magnitude by hydrogen and vacuum reduction
- (h) production of a rust-red coloration by oxidation and a weak



yellow-green coloration by reduction, the coloration appearing throughout the volume of the samples in both cases

- (i) production of an increase in sensitivity to oxygen by roughening the surfaces of a sample
- (j) lowering of dark conductivity and photoresponse by diffusion of indium, a trivalent impurity, into sample.

In addition, the artificial samples showed these effects:

- (a) low conductivity with original surfaces, but relatively high conductivity with surfaces roughened
- (b) high photosensitivity with rise and decay very fast in comparison to those of natural samples
- (c) no measurable dependence of photoresponse on oxygen unless surfaces had been roughened.
- (d) slow rise and decay, with limited sensitivity to oxygen, if surfaces had been roughened
- (e) considerable slowing of photocurrent decay at temperatures below  $240^{\circ}\text{K}$
- (f) peak photoresponse in 310-320  $\text{m}\mu$  wavelength region
- (g) indicated decrease of carrier mobility with decreasing temperature at low temperature
- (h) approximately logarithmic decay of photocurrent under continued illumination after ten to twenty minutes of illumination.

These results and the relationships between certain of them provide a basis for proposing a photoconduction mechanism for stannic oxide. In addition, further evidence for an impurity-band conduction mechanism in the natural samples has come to light, with an extension

of evidence for the artificial samples being the same basic material as the natural samples.

### The Photoconduction Kinetics in Terms of a Chemisorption Process

It was assumed at the outset of the present work that light-induced changes occurring at constant temperature arise solely from changes in carrier density, the mobility remaining constant. The photoconduction in natural specimens has been found to be characterized by logarithmic decay and a strong dependence on the presence of gaseous oxygen. These same features had earlier been observed in sintered samples of zinc oxide. (16). A similar dependence of photoconduction on oxygen has also been found in single crystals of zinc oxide and polycrystalline films of lead monoxide. (10, 11, 15). Collins and Thomas (15) have advanced a theory for zinc oxide photoconductivity based entirely on chemisorption and surface photolysis.

At this point, it would be well to consider the four assumptions listed at the beginning of Chapter II in the light of the experimental results.

The first assumption stated that there should be no hole component of the photoconductivity. The dark conductivity of all samples examined by Hall techniques has been found to be n-type. (26). No Hall or thermoelectric measurements have been undertaken with a sample during any time at which photoexcited carriers might have been present. However, in artificial samples having both original and ground surfaces, a decrease in photocurrent during a long period of illumination was noted. According to Bube (36), this signifies the participation of

only one type of carrier and a lack of replenishment of this carrier at the electrodes. This circumstantial evidence favors n-type photoconductivity, as does the oxygen dependence. Oxygen tends to accept electrons to form negative ions. An adsorbed oxygen ion could therefore become neutralized by trapping a hole. The effect of oxygen on the photoresponse is such that a mechanism of this type most readily provides a satisfactory explanation.

The second assumption was that  $\Delta n/n \gg \Delta q/q$ . Values of  $n$  in the natural stannic oxide samples were customarily near  $10^{14} \text{ cm}^{-3}$ . In a short exposure at ordinary light intensity,  $\Delta n/n = 0.1$ . Consider the sample to be  $1 \times 4 \times 8 \text{ mm}^3$ , with a surface area  $4 \times 6 \text{ mm}^2$  under direct illumination. Then the number of added photocurrent carriers would be  $3.2 \times 10^{11}$ , and under the fourth assumption ( $\Delta N = \Delta Q$ ) the number of oxygen ions desorbed would be the same. To establish orders of magnitude, assume a monolayer of adsorbed oxygen consisting of one ion per surface oxygen site in which case  $q \doteq 2 \times 10^{15} \text{ cm}^{-2}$ . The value of  $\Delta q$  is approximately  $1.3 \times 10^{12} \text{ cm}^{-2}$ , so that  $\Delta q/q = 7 \times 10^{-4}$ , which is much less than  $\Delta n/n$ . If there is only one tenth of a monolayer adsorbed, then  $\Delta n/n = 15 \Delta q/q$ . No values of  $q$  have been measured, but for reasons that will be brought out later, it seems acceptable to assume that there is not more than a monolayer of chemisorbed oxygen on the surface of this material at room temperature.

The third assumption was that processes governing physical adsorption act rapidly in comparison with the electron transfer involved in the basic rate-limiting process. At temperatures above  $99^\circ\text{K}$ , there was an immediate response of the photocurrent to a change in the oxygen pressure, implying rapid physical attachment from which

electron transfer could proceed. The logarithmic behavior with slopes reflecting the availability of gaseous oxygen furnished added evidence that no intermediate processes appreciably retarded the exchange.

The fourth assumption was that of a one-to-one correspondence between the number of desorbed oxygen ions and the number of photoconduction electrons. This assumption was used in the partial justification of the use of the second assumption. The observation of a decay linear with  $\ln(t + t_d)$ , with  $t_d$  a reproducible constant for a given temperature and sample, indicates that  $\Delta N/\Delta Q$  is a constant but does not fix any value.

On the presumption that processes associated with second and further layers would not be identical to those involved in the attachment of the first layer, it may be argued that the effects observed in connection with the photoconductivity of stannic oxide involve a single layer of adsorbed ions -- in view of the rapidity of the changes described above, probably a monolayer or less. Otherwise the constant B of Equation 11 might be expected to alter during the course of a decay.

Although an ironclad justification of all four of the assumptions used cannot be presented on the basis of the experimental results, it nevertheless appears that the decay theory outlined in Chapter II is applicable to the case of stannic oxide. However, all observations indicate that the  $\text{SnO}_2$  surface must be cut before the interplay between chemisorption and photoconduction becomes evident under the experimental physical conditions, i.e., at temperatures between  $120^\circ\text{K}$  and  $320^\circ\text{K}$  and pressures between  $5 \times 10^{-8}$  mm Hg and atmospheric pressure.

It is still not known whether the oxygen ions taking part in the process dealt with here are diatomic or monatomic during the time that they are chemically attached to the surface, nor whether the photolysis of lattice oxygen makes any appreciable contribution. However, it appears possible to explain experimental results without recourse to the latter mechanism.

Under the most intense illumination used, a typical sample would develop a saturation photocurrent corresponding to a  $\Delta q$  of the order of  $10^{13}$   $\text{cm}^{-2}$ , or about 0.01 monolayer, at room temperature. This figure could be increased by reduction of the ambient oxygen pressure, and no lower limit on the pressure producing a noticeable effect was reached in the experimental work. Sample XVII showed evidence of continuing to respond to pressure changes between  $10^{-6}$  and  $10^{-7}$  mm Hg, although more in the photocurrent decay than in the rise. Saturation photocurrents showed the greatest variation with oxygen pressure in sample XIII A, the surface of which had been roughened. Vacuum photocurrents between three and four times the photocurrents measured in air or oxygen at atmospheric pressure were noted in this specimen, apparently because of the increased surface-to-bulk ratio. Typical saturation photocurrent ratios for polished natural samples were in the range between 1.5 and 2.

All natural samples, as well as artificial samples having roughened surfaces, showed the same fundamental shapes of rise and decay curves, although the initial rates of rise and decay were noticeably enhanced in reduced natural samples. Under none of the attainable experimental conditions would the initial rate of rise or decay be reduced to an unmeasurable value. From these observations it is

evident that the same fundamental processes dominate the photoconduction in this material throughout the temperature and pressure ranges employed in the present study.

Approximate values of the chemisorbate density  $q$  can be calculated from data obtained from long exposures during which the photocurrent became saturated, if it is assumed that:

1. there are no photoconduction mechanisms other than the oxygen sorption process taking part,
2. electron trapping in the bulk is negligible,
3. the changes in carrier density are spread throughout the volume of the sample,
4. chemisorbate density changes occur only on the directly illuminated portion of the surface, and
5. the photodesorption rate term  $L$ , instead of remaining constant as was assumed in the development in Chapter II, actually varies linearly with the chemisorbate density  $q$ .

Equation 9b would then take the form

$$\frac{dq}{dt} = a \exp(-bq) - cq \quad (28)$$

where  $c$  is a constant embodying the dependence on light intensity.

Then for the case of saturated photocurrent flowing under constant illumination, the photodesorption rate would be  $-cq$ , and the readsorption rate  $cq$ . Also, the adsorption rate at the instant the photocurrent decay begins, assuming the influx of radiant energy to become zero instantaneously, would be this same quantity. This rate is known for the decays following many extended exposures.

Consider the results obtained from long exposures to ultraviolet illumination at high intensity of sample IV. Calculated values of

$\Delta q = q_e - q_f$  in oxygen-rich ambients ranged from  $5.0 \times 10^{12} \text{ cm}^{-2}$  to  $7.1 \times 10^{12} \text{ cm}^{-2}$ . The value of the geometrical factor  $x_0$  for this series of experiments was 0.4 cm. Take a typical value of  $\Delta q$  at saturation to be  $6 \times 10^{12} \text{ cm}^{-2}$  for this sample and light intensity. Similar runs using the same sample and illumination in helium and vacuum showed that the ratio of saturation photocurrent in an essentially oxygen-free ambient to that in an oxygen-rich ambient is generally near 1.5. Comparisons of the initial decay slopes measured for these same runs showed that observed in oxygen to be about 6.5 times that in vacuum or helium.

Since

$$\left(\frac{dq}{dt}\right)_{t=0} = cq_f \quad (29)$$

is the instantaneous rate measured, then the ratio of rates in two different ambients is also the ratio between values of  $q_f$  for the same two ambients. From the previous paragraph, then, the  $q_f$  in an oxygen-rich ambient is about 6.5 that in an oxygen-free ambient. This and the ratio of saturation photocurrents give two equations involving  $q_f$  and  $q_e$ , which are

$$q_f(\text{oxygen}) = 6.5 q_f(\text{vacuum}) \quad (30)$$

and

$$(q_e - q_f)(\text{vacuum}) = 1.5(q_e - q_f)(\text{oxygen}) \quad (31)$$

Resulting values of  $\Delta q/q_e$  are 0.94 and 0.63 for vacuum and oxygen respectively. With  $\Delta q(\text{vacuum}) = 9 \times 10^{12} \text{ cm}^{-2}$ , the corresponding value of  $q_e$  is  $9.5 \times 10^{12} \text{ cm}^{-2}$ .

Similar calculations carried out using the rise and decay slopes at  $t = 0$  and  $t = 0$  respectively from single experiments, gave values

of  $q_e$  between  $5.5 \times 10^{12} \text{ cm}^{-2}$  and  $8 \times 10^{12} \text{ cm}^{-2}$ , but the associated values of  $\Delta q/q_e$  for oxygen-rich ambients were unreasonably high, near 0.9. For this reason the results in the above paragraph are believed to provide a more nearly accurate estimate of  $q_e$ . Furthermore, there is no necessity to ascribe the same constant ratio to  $L/q$  at the beginning of illumination and the photocurrent saturation time.

These decay rate ratios also provide a means of estimating an "average"  $b$ , since if the pressure variation of the physically adsorbed oxygen coverage is neglected, one obtains at  $t = 0$ ,

$$\frac{\frac{dq}{dt} \text{ (oxygen)}}{\frac{dq}{dt} \text{ (vacuum)}} = \frac{\exp[-bq_f \text{ (oxygen)}]}{\exp[-bq_f \text{ (vacuum)}]} \quad (32)$$

For the case cited, the resulting value of  $b$  is  $6.2 \times 10^{-13} \text{ cm}^2$ . This and associated quantities will be covered in greater detail shortly.

The values of  $q_e$  calculated above, being no more than one per cent of a monolayer, indicate that the chemically adsorbed oxygen becomes attached at surface sites varying from the energetic norm by virtue of an impurity atom or ion, a structural defect, or a surface configuration of some unusual nature.

These values of  $\Delta q/q$  may cast doubt on the validity of the second assumption used in the theoretical development. If the fourth assumption continues to hold true, then both  $\Delta n/n$  and  $\Delta q/q$  are approximately equal, having maximum values near unity. The assumption that the fractional change in carrier density is much larger than the corresponding change in chemisorbate concentration allowed the linearization of  $E(q)$ . If this simplification cannot be employed, then a variation



of  $C_a$  with  $q$  becomes important. The time factor is also of some importance in these considerations, inasmuch as restricting carrier density changes to values an order of magnitude or more below the saturation value may yet permit the use of a constant  $C_a$  in the computations. This can be tested in principle by calculating the barrier height change  $\Delta E$ ,  $C_a$ , and the barrier layer thickness  $d$  using data obtained from the rise and decay curves resulting from an exposure of short duration.

If Equation 8, which is the linear relationship between  $E(q)$  and  $q$ , is rewritten as a difference equation, it takes the form

$$\Delta E = e^{\beta} \Delta q / C_a \quad (33)$$

with  $C_a$  constant. From the definition of the constant  $b$ ,  $e^{\beta} / C_a = kTb$ . Also,  $\Delta q = x_0 \Delta n$  (Equation 10) and  $b = Bx_0^{-1}$  (definition of  $B$ ). With these substitutions Equation 32 becomes

$$\Delta E = kTB\Delta n \quad (34)$$

in which  $\Delta n$  is obtainable from photocurrent curves if the assumption that mobility is not affected by illumination is again used. The constant  $B$  can be obtained from the slopes of logarithmic decay curves, which have been plotted as  $\Delta n / \Delta n_0$  vs.  $\ln(t + t_d)$ . From Equation 17, the slope of such a plot is seen to be  $(B\Delta n_0)^{-1}$ .

The slopes of logarithmic decay curves resulting from one-minute exposures using sample IV are given in Table X. The room temperature value of  $(B\Delta n_0)^{-1}$  is 0.12, which with a  $\Delta n_0$  of  $8 \times 10^{12} \text{ cm}^{-3}$  gives a  $B$  of roughly  $1 \times 10^{-12} \text{ cm}^3$ . At room temperature,  $kT = 0.025 \text{ eV}$ , and if the entire rise is considered, then  $\Delta n = \Delta n_0 = 8 \times 10^{12} \text{ cm}^{-3}$ . Therefore, the barrier height change for this case is approximately 0.2 eV. Taking the sample volume and area illuminated as the geometrical

factors of interest, the value of  $x_0$  for this case is 0.13 cm. This gives a value for  $b$  of  $8 \times 10^{-12}$  cm<sup>2</sup>, which in turn leads to  $C_a = 0.8$   $\mu\text{f}/\text{cm}^2$ , using  $C_a = e^2/bkT$ . If the static dielectric constant for stannic oxide is taken to be 24, as reported by Berberich and Bell (37), this capacitance per unit area corresponds to a barrier layer thickness of about  $5 \times 10^{-6}$  cm. Note that here the directly calculated value for  $b$  is an order of magnitude greater than that calculated from decay slope ratios of long exposures involving the same sample with pressure dependence of the physically adsorbed oxygen coverage neglected.

This discrepancy in the values of  $b$  may also be due to changes taking place within the sample as a result of extended periods of illumination. The outstanding possibility is alteration of the barrier layer capacitance per unit area,  $C_a$ . The direction of change seems to be well established, although relative magnitudes are not in complete agreement. The values of  $B$ , which are directly proportional to those of  $b$ , have been calculated for decays resulting from exposures having durations of 5 minutes and 500 minutes, also involving sample IV in oxygen at room temperature, but with a reduced light intensity. Pertinent figures are given in Table XV.

TABLE XV  
PARAMETERS ASSOCIATED WITH CALCULATION OF  $B$   
(SAMPLE IV)

Exposure time (min)	$\frac{\Delta n_f}{n_s}$	$\frac{\Delta n_f}{(\text{cm}^{-2})}$	$(B\Delta n_f)^{-1}$	$B$ (cm <sup>-3</sup> )
5	1.018	$1.8 \times 10^{12}$	0.045	$12.4 \times 10^{-12}$
500*	1.057	$5.7 \times 10^{12}$	0.032	$4.7 \times 10^{-12}$

\*Photocurrent reached saturation

In this case  $b$  shows a decrease by a factor of 2.6, as compared to an order of magnitude in the earlier example. It is not certain whether the light intensity is an influential factor in the changes indicated by these estimates. However, all variations of  $b$  are consistent with increased surface "cleaning" associated with longer exposures or higher light intensities. This would be expected to reduce the magnitude of  $q_f$ , reducing  $d$  and increasing  $C_a$ .

If Equation 32 is now modified to take into account the possibility of a variation of  $q_p$  with the oxygen pressure, as

$$\frac{\left(\frac{dq}{dt}\right) (0)}{\left(\frac{dq}{dt}\right) (V)} = \frac{q_p (0)}{q_p (V)} \exp[-bq_f (0) + b'q_f (V)] \quad (35)$$

where it has been assumed that other factors entering into the coefficient  $A$  are not affected, the notations (0) and (V) refer to oxygen and vacuum respectively, and values of  $b$  and  $b'$  calculated from the slopes of logarithmic decay curves are used, the relationship linking  $q_p (0)$  and  $q_p (V)$  can be sought. If this is done for similar long exposures involving sample IV in which the photocurrent reached saturation, it is found that the ratio of the two  $q_p$ 's is of the order of ten,  $q_p (0)$  being the larger. This is far from being in agreement with a linear dependence on the oxygen pressure as predicted by elementary physical adsorption theory, inasmuch as the corresponding pressure variation covers approximately eight orders of magnitude. This seems to indicate that the physical adsorbate does not achieve equilibrium with the ambient at a rate compatible with the rate of conversion between the two types of adsorption.

The estimated values of the parameters associated with the barrier

layer cited for the case of one-minute exposures are reasonable, indicating that the treatment described cannot easily be ruled out for the case of a short exposure at room temperature. Furthermore, several factors used here may be in error. Foremost among these are the values of the dielectric constant and of  $x_0$ . It is not known how much the surface layer value for the dielectric constant varies from the bulk value. Also, the value of  $x_0$  may be too large by a factor possibly as large as five since the measured area was based on a plane surface, while the effective surface area is larger depending on roughness on a scale beyond the available means of optical observation. A more accurate value of  $x_0$  would give a larger  $b$ , a smaller  $C_a$ , a larger  $d$ , and a smaller  $\Delta q/\Delta n$  ratio. This improves the validity of the  $\Delta q/q \ll \Delta n/n$  assumption.

The earlier analysis can be used to evaluate  $A'$  and  $A$ , since  $Bn_f A' = t_d^{-1}$ . For the same experimental case involving a short period of exposure the measured value of  $t_d$  was 2.3 sec and that of  $n_f$  was  $1.08 \times 10^{14} \text{ cm}^{-3}$ , giving  $A' = 4 \times 10^{-3} \text{ sec}^{-1}$  and  $A = A'n \doteq 4 \times 10^{11} \text{ cm}^{-3} \cdot \text{sec}^{-1}$ ,  $n$  having remained near  $10^{14} \text{ cm}^{-3}$ .

Turning to lower temperatures, the use of this method is beset by several problems, among them the lack of carrier density data. Of greater interest, however, are the changes which take place in the shape of the decay curve and the decreased dependence on ambient oxygen. Both of these effects point to a decrease in the rate of physical desorption of chemically desorbed oxygen as the temperature is lowered. This is further evidenced by the lessening of the initial decay rate with increasing time of exposure at low temperatures which, along with the comparatively small oxygen dependence, shows that a reduced amount

of physical desorption continues to take place even near the liquefaction point of oxygen (see Figures 11 and 16, Table IX). This is in qualitative accord with a general thermal picture of physical adsorption, and indicates physical desorption energies of the order of hundredths of an electron volt.

From Chapter II, the chemisorption rate is linearly dependent on the concentration  $q_p$  of the physically adsorbed species. At room temperature this is essentially a dependence on the oxygen pressure and a sticking coefficient, but as the temperature decreases the results imply that a pressure-independent component of  $q_p$  comes into play and finally becomes the factor dominating the chemisorption process. Or in other words, at lower temperatures the time required for the concentration of physically adsorbed oxygen to achieve equilibrium with the ambient is greatly increased.

The same general model is applicable to the case of artificial samples on which the surfaces have been roughened. These show behavior at room temperature highly similar to that of the natural samples, including the oxygen dependence of saturation photocurrent and a logarithmic decay rate which is also dependent on the oxygen pressure. However, the greatly different conduction and photoconduction characteristics observed in artificial specimens retaining their original surfaces show that a somewhat different surface must be considered if the chemisorption model is to be extended to these samples. One element of the photoconductive behavior associated with the grown surfaces which can be correlated directly with that of the mechanically altered surfaces is the wavelength dependence of photoresponse. A moderately slow photocurrent rise curve also is noted, but saturation

is reached in considerably less time and there is no measurable oxygen dependence. The decay of photocurrent under continued illumination in an exposure extending over a period of at least several minutes indicates, according to Bube (36), that only one sign of carrier is mobile. Although this does not indicate whether the carriers in this case are holes or electrons, it is in at least partial agreement with the first assumption stated at the outset of the development in Chapter II, which permits only one sign of photocurrent carrier and in addition specifies that this carrier must be of negative sign.

The slowing of photocurrent decay with decreasing temperature in samples having grown surfaces shows that a potential barrier lies between the bulk of the carriers participating in the photoconduction process and the recombination sites. In the chemisorption model the surface layer forms such a barrier, opposing the flow of electrons to the surface. In the case under consideration a barrier height of several hundredths of an electron volt is indicated.

In the natural samples the faster photocurrent decays at lowest temperatures were explained in terms of physically adsorbed oxygen. This suggests a cause for the rapid decays seen at room temperature with the grown surfaces, which in turn provides a basis for analyzing the behavior of these surfaces in terms of the chemisorption model.

Since the coefficient  $a$  is by definition linearly dependent on the carrier density  $n$  and the concentration  $q_p$  of the physically adsorbed species, let  $a = \gamma n q_p$ , so that Equation 9a becomes

$$\frac{dq}{dt} = \gamma n q_p \exp(-bq) \quad (36)$$

where  $n$  and the chemisorbate density  $q$  are time-dependent quantities.

Since in these samples the dark current is two to three orders of magnitude less than the saturation photocurrent, the carrier density  $n(t)$  can be considered to consist of only the photoexcited carrier density, and the fraction of the remaining photocurrent at time  $t$  during a decay is then equal to  $n(t)/n_s$ , where  $n_s$  is the carrier density at saturation. Let  $q_0$  be the total concentration of adsorbed oxygen, both chemically and physically bound. In the dark, then,  $q_0 = q_c + q_p$ . The physically attached oxygen density  $q_p$  may be dependent upon both the pressure of the ambient and time, the latter variation arising from a possible difference between the rate of conversion by incident radiation of chemisorbed oxygen to physically adsorbed oxygen and the rate at which the physical adsorbate can attain equilibrium with the ambient. It is not known whether the sites associated with physically adsorbed oxygen converted by light from chemisorbed oxygen are distinct from those associated with oxygen physically adsorbed as a normal consequence of the contact of the surface with the ambient. It is evident, however, that at room temperature and lower temperatures a considerable density of recombination sites is readily available and that there is no noticeable pressure effect on the chemisorption rate. These general bits of experimental information indicate that either there is an equilibrium physical adsorbate concentration exceeding--possibly by an appreciable factor--the chemisorbate density and having sites indistinguishable from the sites associated with chemically desorbed oxygen remaining physically attached, or that, independent of the physical adsorbate density in the dark, essentially all chemically desorbed oxygen remains physically adsorbed during the period of illumination. In either case,  $q_0$  may be assumed to remain

constant, so that for a decay during which the pressure is not changed  $q_p(P, t) = q_0 - q(t)$ .

With this, the decay equation can be written

$$\frac{dq(t)}{dt} = \gamma n_f \left[ \frac{n(t)}{n_f} \right] \left[ q_0 - q(t) \right] \exp[-bq(t)] \quad (37a)$$

which for the first case, that for which  $q_0 \gg q_e$ , is equivalent to

$$\frac{dq(t)}{dt} = \gamma n_f q_0 \left[ \frac{n(t)}{n_f} \right] \left[ 1 - \frac{q(t)}{q_0} \right] \exp[-bq(t)] \quad (37b)$$

and for the second case, using  $q_0 \doteq q_e$ , becomes

$$\frac{dq(t)}{dt} = \gamma n_f (q_e - q_f) \left[ \frac{n(t)}{n_f} \right]^2 \exp[-bq(t)] \quad (37c)$$

since  $\frac{q_e - q(t)}{q_e - q_f} = \frac{n(t)}{n_f}$ .

Consider Equation 37b, which with  $q_p \gg q_e$  reduces to

$$\frac{dq(t)}{dt} = \gamma n_f q_0 \left[ \frac{n(t)}{n_f} \right] \exp[-bq(t)] \quad (38)$$

in which the quantities  $dq/dt$  and  $n/n_f$  are obtainable from any sufficiently slow decay curve, such as those resulting from low temperature measurements. Such curves, being of the same general shape as the 30-millisecond decay curves seen at room temperature in the same sample and the decay curves observed in natural samples at low temperatures following a short period of illumination (see lower curve in Figure 16), are believed to be representative of the adsorption-influenced process under consideration here.

Several decay curves for sample GI have been examined after the initial fast portion in terms of the above quantities, to reveal any trends which might favor the application of either Equation 37c or Equation 38. To simplify notation, let  $S = di/dt \propto dq/dt$  and let  $F = n/n_f$ . These and related quantities have been listed below in



Table XVI for several data points taken from the decay curve of sample GI at 190°K.

TABLE XVI  
VARIATION OF F AND S FOR SAMPLE GI AT 190°K

F	S	S/F	ln(S/F)	S/F <sup>2</sup>
0.09	0.21	2.3	0.833	25.6
0.10	0.31	3.1	1.131	31.0
0.13	0.49	3.8	1.335	29.2
0.16	0.70	4.4	1.481	27.5
0.20	1.22	6.1	1.808	30.5
0.23	1.56	6.8	1.917	29.5

Results of the same general nature were obtained from decay curves for which the temperature was lower, the lowest being 122°K. At temperatures above 200°K, more scatter appears in the values of SF<sup>-2</sup>. Values of the ratio of the highest value of SF<sup>-2</sup> to the lowest are 1.13, 1.21, 1.64, and 1.57 at 133, 190, 208, and 222°K, respectively. The random character of the scatter, along with the fact that it increases with increasing temperature (increasing rate of decay), strongly indicates that it arises from reduced precision associated with measurements of smaller quantities.

That SF<sup>-2</sup> shows a tendency to remain essentially constant as F varies, while there is no obvious simple relationship between S/F or ln(S/F) and F, shows not only that Equation 37c with its attendant relationships between carrier densities and adsorbate densities is the more suitable expression for describing these decays, but that the exponential factor is relatively unimportant (note that earlier results indicate b and q change in the same direction). This in turn implies

both that the fraction of chemisorbate "cleaned" off the surface is small and that the oxygen which is chemically desorbed remains physically attached. Furthermore, this indicates that the sites on which chemically desorbed oxygen is physically held are in some manner different from those involved in the usual physical adsorption arising from the contact between surface and ambient. A question that is not answered, however, is whether there is any exchange between the two types of physical adsorption sites, i.e., whether those oxygen atoms (or molecules) which have been chemically desorbed by the action of the incident radiation are free to migrate along the surface, subject to replacement by other physically adsorbed oxygen, or are "locked" in their respective sites. The temperature dependence of the decay rates shows that the assumed surface barrier layer is influential in the photoconduction process in the grown samples having their original surfaces, and hence that a surface mechanism can be responsible for the photoconductive behavior in these samples as is the case with those having mechanically altered surfaces. A chemisorption mechanism is favored over a photolysis mechanism despite the absence of a measurable oxygen pressure dependence.

No values of  $q$  could be calculated for the grown samples having their original surfaces, there being no applicable carrier density data available. If these samples are taken to have a dark conductivity of  $10^{-6} \text{ ohm}^{-1} \text{-cm}^{-1}$  and a carrier mobility of  $100 \text{ cm}^2/\text{V-sec}$ , the carrier density would be  $6 \times 10^{10} \text{ cm}^{-3}$ . Corresponding saturation values of  $\Delta n$  and  $\Delta q$  would then be approximately  $10^{13} \text{ cm}^{-3}$  and  $10^{11} \text{ cm}^{-2}$ , respectively, for a typical case at room temperature.

That grown surfaces and cut surfaces should have different

time rates associated with their behavior, particularly at high temperatures, is not surprising when the possibility of different types of sites arising from the different methods of surface preparation is taken into account. A grown surface tends to incorporate only crystallographic planes which provide for a minimum surface potential energy under the conditions of growth, while a cut surface--particularly in a material like stannic oxide which does not show well-defined cleavage--will contain other planes and hence different types of adsorption sites. This, of course, points to the likelihood of different energies for physical desorption in the two cases.

A summation of the relationship between the surface behavior and the photoconductivity is illustrated by Figures 20(a), 20(b), and 20(c) (see page 100). Inasmuch as ground and polished natural samples at room temperature were the most thoroughly studied, the model chosen for the discussion is based on this situation. The chief differences between this model and one that would be more suitable for the artificial samples or low temperature behavior lie in the amounts of physical desorption taking place.

Figure 20(a) depicts the energy bands at and near the surface of a natural sample in the dark at room temperature. Oxygen chemisorbed on the surface in the form of  $O^-$  or  $O_2^-$  holds a net negative charge on the crystal surface, with the consequence that a depletion layer is formed. In the dark, conductivity is n-type and takes place primarily within the bulk. The surface potential has a height  $\phi_0$  as defined by the picture.

In Figure 20(b) an ultraviolet photon is absorbed to create a hole-electron pair near the surface. The electric field existing in

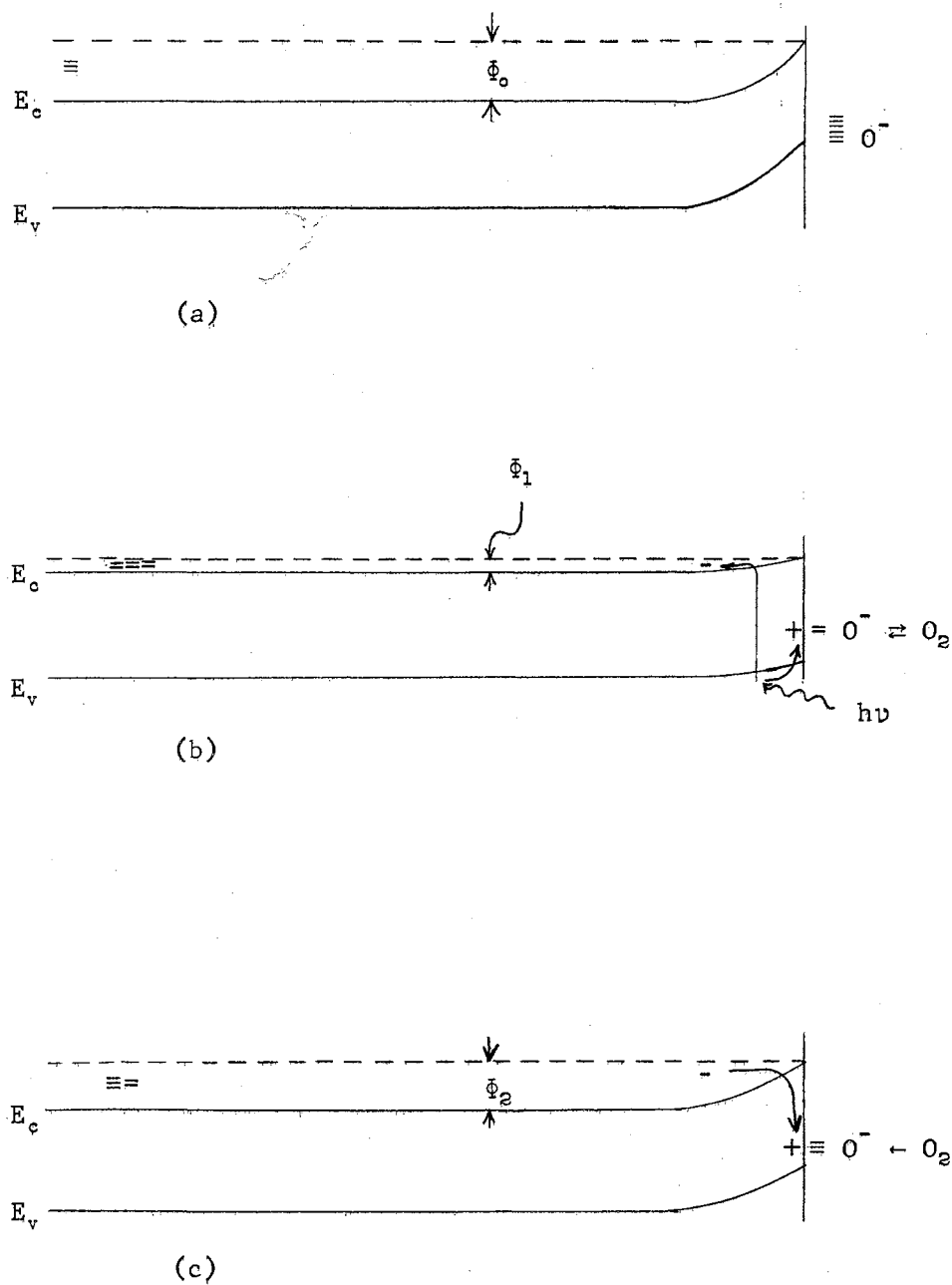


Figure 20. Influence of Photoconduction on Surface Energy Bands in Stannic Oxide

the barrier layer causes the electron to move into the bulk while the hole is drawn to the surface. There the hole combines with and neutralizes a chemisorbed oxygen ion leaving the electron produced with the hole by the photon absorption in the conduction band in the bulk. This increases the carrier density and hence the conductivity. The reduction of the net negative charge density at the surface results in a decrease in the height of the potential barrier, so that  $\phi_1 < \phi_0$ . The chemically desorbed oxygen is free to become physically desorbed and with a saturated photocurrent there is a balanced exchange of electrons between the crystal surface traps and the bulk.

In Figure 20(c) illumination has recently been discontinued and decay is in progress. Because of the reduced surface potential, conduction electrons can more easily approach the surface where they may possibly recombine with a hole-oxygen atom (or molecule) configuration to form a chemisorbed oxygen ion. As this recombination progresses at a rate determined by the concentration of physically adsorbed oxygen at the surface, the excess conductivity decays and the barrier potential increases,  $\phi_2$  approaching  $\phi_0$  as the decay nears completion.

Measurements of the dark conductivity and the contact potential indicated that there is no appreciable reaction between the stannic oxide surface and ambient oxygen without excitation by ultraviolet light. Tests with air and oxygen bubbled through water failed to produce a catalytic effect like that observed in single crystals of zinc oxide. (15). The pressures at which the greatest oxygen-induced changes in the photoconductivity of natural stannic oxide occur lie between  $10^{-2}$  and  $10^1$  mm Hg. An upper limit appears to lie below 150 mm Hg, but no lower limit has been found.

### Effects of Oxidation and Reduction

The results of oxidation and reduction were strange in that both produced a permanent lowering of the dark conductivity, the latter by a considerably larger factor. This rules out the dominance of an oxygen vacancy mechanism in the electrical conductivity of natural stannic oxide. The colorations produced in the samples used in these experiments not only indicate the presence of impurities, but show that a change in the state of ionization may have occurred in one or more impurities. A valence change in a transition metal impurity would suffice to explain both the coloration and conductivity changes. This reinforces earlier findings that natural samples may show some impurity-band conduction. (26).

Surface erosion in a hot hydrogen atmosphere is most likely due to the decomposition reaction



with the subsequent evaporation of excess tin.

The very high surface resistance measured in sample VIII B and the sharp rise and decay of photocurrent observed in samples VIII A and VIII B suggest that the surfaces of these samples were affected by heat so as to more nearly approach the configuration of a grown surface.

No important changes in optical transmission or the wavelength distribution of photoresponse were observed in either oxidized or reduced samples.

### Effects of Indium Diffusion

The decrease in conductivity observed in a specimen into which

indium metal had been diffused can be interpreted as being due either to the effects of heating or to the action of a trivalent impurity, which in a substitutional position would be expected to act as an acceptor and thus reduce the conductivity of an n-type material such as the stannic oxide used in the experiments described.

The reduction of photosensitivity, however, indicates the indium produced some alteration in the surfaces of the two samples used. While the basic character of the photocurrent rise and decay was not appreciably changed, the wavelength shift of the photoresponse peak in sample II points to the addition of a step in the processes linking photon absorption and the entry of a photocurrent carrier into the conduction band. The fact that the peak is located at the same wavelength as the short wavelength cutoff is significant, suggesting the possibility of indirect optical transitions and an energy gap of a somewhat greater width than had previously been thought for these samples. The larger energy gap, near 3.9 eV, could then involve direct optical transitions, while the smaller apparent "gap," near 3.5 eV, would result from the indirect transitions. An indirect transition is one in which a lattice phonon enters into the absorption or emission of a photon and brings an energy difference, not always evident in elementary optical measurements, into the process. Such phonons may be either absorbed or emitted in this kind of a transition.

#### Suggestions for Further Study

Several questions, relating to both surface properties and more general features, have arisen during the course of the present study of stannic oxide. Probably among the most important is the apparent



ambiguity in the measured values for the energy gap. Measurements of the reflectivity, along with a detailed determination of the absorption coefficient as a function of wavelength in very thin monocrystalline plates in the near ultraviolet region of the spectrum, would reveal the presence of indirect transitions. A more detailed determination of the wavelength distribution of photosensitivity over a continuous range between 250 and 400  $\mu$  might furnish additional useful information.

More precise knowledge of the general properties of the artificial samples is needed. This includes measurements of the conductivity and Hall mobility as a function of temperature, direction of Hall emf, and optical characteristics. Also needed is a determination of the impurity content of these samples, and their reactions to oxidation and reduction experiments.

A comparison, possibly by a field emission technique, of the surface structures of samples retaining their original surfaces and of samples which have been subjected to any form of surface abrasion should be very helpful in ascertaining the fundamental reason for the striking differences in the behaviors observed. Such a technique would also provide a means for a more direct observation of sorption processes.

The actual amount of oxygen physically desorbed might be measured by either of two high vacuum methods. Probably the simplest of the two would be by determination of pressure changes brought about by ultraviolet irradiation of a sample enclosed in a small high vacuum chamber of known volume. Such measurements could be made concurrently with photoconduction measurements and the results of the two correlated. The other method would employ a vacuum microbalance and high surface-area powder samples. The nature of such a measurement would almost certainly



rule out the simultaneous determination of any electrical parameter but could furnish highly accurate data on the amount, and conceivably the surface concentration, of physically detached material.

A comparison of the results of experiments similar to those described in the present study, but with stannic oxide crystals having atomically clean surfaces, should be highly informative. In particular, it should settle the question of whether photolysis--the detachment of lattice atoms or ions under illumination of sufficiently short wavelength--occurs in this material. Supposedly such surfaces could be obtained by cleavage or by bombardment with ions of an inert gas, either of these operations necessarily being done in ultrahigh vacuum.

Several types of contact potential measurements other than those performed are obviously needed. Foremost among them is the determination of the change in the height of the potential barrier under direct ultraviolet illumination, which would necessitate the use of a grid-type reference electrode. An ambient which might prove to be of interest in measurements of both the contact potential and the dark conductivity is atomic oxygen, which could most readily be supplied by the breakdown of ozone produced by a spark gap within the system near the sample. Very strict temperature stabilization of sample and apparatus, along with the use of more sensitive instrumentation, might also reveal slight ambient effects due to diatomic oxygen on contact potential and dark conductivity. Temperature tolerances would have to be to within  $0.1^{\circ}\text{K}$  or less, and the change in barrier height expected should not exceed 0.01 V at room temperature.

A more specific knowledge of the ionic character of the chemically adsorbed species might be revealed by a study of the paramagnetism

associated with the stannic oxide surface under various conditions and further chemical variation of the ambient may also prove to yield detailed information of this nature. Gaseous compounds containing oxygen could produce effects indicating catalysis. Among a wide assortment of such compounds only water vapor has yet been tested. Other reactions might be induced by the presence of halogens, with their high electron affinity.

The employment of AC methods in the various types of photoconductivity measurements might provide a sensitivity of detection which would be particularly important in temperature and wavelength distribution work. The value of such techniques in ambient work would depend on physical sorption characteristics.

Knowledge of low temperature mobilities and carrier densities, as well as values of the surface mobility and carrier density at all temperatures, is still lacking. In view of surface mobility effects discussed by Schrieffer (38) such measurements could prove to be of value in the development of an all-inclusive picture of the stannic oxide surface.

A means of more closely examining one of the important assumptions used in the present work, that of unchanging carrier mobility under varying illumination, has been proposed by Bube and MacDonald (39) in the form of Photo-Hall measurements. Such measurements reveal not only mobility changes induced by the illumination which produces photoconductivity but detect changes in the relative densities of the two signs of current carriers due to this illumination. Techniques for Photo-Hall measurements in materials having conductivities as low as  $10^{-10} \text{ ohm}^{-1} \text{ -cm}^{-1}$  have been developed. (40).

Whether the oxygen sorption phenomena discussed here are common to all oxide semiconductors or occur only in specific compounds has yet to be determined. A parallel study of rutile--tetragonal titanium dioxide--would be of great interest, inasmuch as this compound is a near twin to stannic oxide with the important difference that conduction takes place in a narrow 3d-band as opposed to the broad-band conduction observed in both stannic oxide and zinc oxide. The behavior of tetragonal lead dioxide should also prove to be of considerable significance, as could that of some of the more complex oxides such as the titanates. An improved understanding of the surface electrical behavior of oxide materials is important in advancing the technology of specialized fields such as catalysis where they already find wide application.

An investigation which bears a special relationship to the work described herein is now under way in this laboratory. Field effect studies designed to provide additional verification of the conclusions reached in this report are in progress. It is hoped that they will give independent data on surface potentials along with energies and densities of trapping states.

## BIBLIOGRAPHY

1. Brattain, W. H., and Bardeen, J., Bell System Tech. J. 32, 1 (1953).
2. Handler, P., Semiconductor Surface Physics, Ed. R. H. Kingston. Philadelphia: University of Pennsylvania Press (1957).
3. Statz, H., and De Mars, G. A., Phys. Rev. 111, 169 (1958).
4. Morrison, S. R., Phys. Rev. 114, 437 (1959).
5. Handler, P., and Portnoy, W. M., Phys. Rev. 116, 516 (1959).
6. Margoninski, Y., Phys. Rev. 121, 1282 (1961).
7. Margoninski, Y., and Farnsworth, H. E., Phys. Rev. 123, 135 (1961).
8. Albers, W. A., Jr., J. Phys. Chem. Solids 23, 1249 (1962).
9. Kennedy, D. R., Ritchie, M., and MacKenzie, J., Trans. Faraday Soc. 54, 119 (1958).
10. Izvozhikov, V. A., Sov. Phys. Solid State 3, 2344 (1961).
11. Bigelow, J. E., and Haq, K. E., J. Appl. Phys. 33, 2980 (1962).
12. Miller, P. H., Jr., Proceedings of the Photoconductivity Conference Held at Atlantic City Nov. 4-6, 1954, Ed. R. G. Breckenridge. New York: John Wiley and Sons, Inc. (1956).
13. Morrison, S. R., Advances in Catalysis, Vol. VII, Ed. W. G. Frankenburg, V. I. Komarewsky, and E. K. Rideal. New York: Academic Press, Inc. (1955).
14. Melnick, D. A., J. Chem. Phys. 26, 1136 (1957).
15. Collins, R. J., and Thomas, D. G., Phys. Rev. 112, 388 (1958).
16. Medved, D. B., J. Chem. Phys. Solids 20, 255 (1961).
17. Deville, H. St. C., Compt. Rend. 53, 161 (1861).
18. Marley, J. A., and MacAvoy, T. C., J. Appl. Phys. 32, 2504 (1961).
19. Ecklebe, F., Neues Jahrbuch Mineral. Geol., Beil. Bd. 66A, 47 (1933).

20. Berton, A., Compt. Rend. 207, 625 (1938).
21. Foex, M., Bull. Soc. Chem. France 11, 6 (1944).
22. Fischer, A., Z. Naturforschung 9a, 508 (1954).
23. Ishiguro, K., Sasaki, T., Arai, T., and Imai, T., J. Phys. Soc. Japan 13, 296 (1958).
24. Northrip, J. W. II, Master's Thesis, Oklahoma State University, 1958 (Unpublished). Pertinent excerpts found in Annual Summary Report (1959), Office of Naval Research Contract No. Nonr-2595(01).
25. Belski, A. J., Master's Thesis, Oklahoma State University, 1960 (Unpublished). Included in the Annual Summary Report (1960), Office of Naval Research Contract No. Nonr-2595(01).
26. Tolly, E. E., Master's Thesis, Oklahoma State University, 1962 (Unpublished). Pertinent excerpts found in Technical Report (1962), Office of Naval Research Contract No. Nonr-2595(01).
27. Hurt, J. E., Master's Thesis, Oklahoma State University, 1959 (Unpublished). Included as an appendix in Annual Summary Report (1959), Office of Naval Research Contract No. Nonr-2595(01).
28. Kohnke, E. E., J. Phys. Chem. Solids 23, 1557 (1962).
29. Frederikse, H. P. R., and Hosler, W. R., National Bureau of Standards Report 6585 (1959).
30. Krusemeyer, H. J., Phys. Rev. 114, 655 (1959).
31. Cronemeyer, D. C., Phys. Rev. 87, 876 (1952).
32. Kronig, R. de L., and Penney, W. G., Proc. Roy. Soc. 130A, 499 (1931).
33. Tamm, I., Physik Zeits. Sowjetunion 1, 733 (1932).
34. Shockley, W., Phys. Rev. 56, 317 (1939).
35. Bardeen, J., Phys. Rev. 71, 717 (1947).
36. Bube, R. H., Photoconductivity of Solids. New York: John Wiley and Sons, Inc. (1960).
37. Berberich, L. J., and Bell, M. E., J. Appl. Phys. 11, 681 (1940).
38. Schrieffer, J. R., Phys. Rev. 97, 641 (1955).

39. Bube, R. H., and MacDonald, H. E., Phys. Rev. 121, 473 (1961).
40. MacDonald, H. E., and Bube, R. H., Rev. Sci. Inst. 33, 721 (1962).

VITA

James Edward Hurt

Candidate for the Degree of

Doctor of Philosophy

Thesis: SURFACE EFFECTS IN STANNIC OXIDE CRYSTALS

Major Field: Physics

Biographical:

Personal Data: Born at Newton, Kansas, February 11, 1935, the son of W. Ernest and Pauline B. Hurt.

Education: Attended grade school in Kiowa and Labette, Kansas, and in Coweta, Atoka, and McAlester, Oklahoma; graduated from McAlester High School in 1953; received the Bachelor of Science degree from the Oklahoma State University, with a major in Physics, in May, 1957; received the Master of Science degree from the Oklahoma State University, with a major in Physics, in May, 1959; completed requirements for the Doctor of Philosophy degree in May, 1963.